Editors' Suggestion

Overhauser dynamic nuclear polarization in alkali metals

Bernardine L. D. Rinkel,[1,*] Katharina Märker,[1,2] Marie Juramy,[1,3] Subhradip Paul,[2,4] Svetlana Menkin,[1,3] and Clare P. Grey[1,3]

[1]*Yusuf Hamied Department of Chemistry, University of Cambridge, Cambridge CB2 1EW, United Kingdom*
[2]*Univ. Grenoble Alpes, CEA, IRIG, MEM, Grenoble 38000, France*
[3]*The Faraday Institution, Quad One, Harwell Science and Innovation Campus, Didcot OX11 0RA, United Kingdom*
[4]*School of Physics and Astronomy, University of Nottingham, University Park, Nottingham NG7 2RD, United Kingdom*

(Received 14 January 2025; revised 20 May 2025; accepted 1 July 2025; published 6 August 2025)

Dynamic nuclear polarization (DNP) of the ^{7}Li NMR lithium metal signal via an Overhauser mechanism was predicted and demonstrated over 70 years ago, and applied more recently at high fields and room temperature to study electrodeposited microstructural lithium metal. Here we further explore the requirements and limitations of the Overhauser effect for alkali metals. Following a theoretical treatment of the Overhauser mechanism, we explain why only relatively modest enhancements are obtained (∼50 compared to a theoretical maximum of 1700 for ^{7}Li) at a magnetic field strength of 9.4 T. Through a systematic investigation of the ^{7}Li enhancement as a function of experimental parameters (magnetic field strength, B_0, temperature, microwave power, and MAS frequency), we show that the experimental enhancements are limited by the short spin-lattice relaxation times (T_{1e} and T_{2e}) of the electrons in lithium metal, and thus the degree of saturation of the electron spin resonance (ESR) transition. The enhancements of ^{6}Li and ^{23}Na are similarly limited by the degree of electron spin saturation, the effect being more pronounced for ^{23}Na; enhancements are improved by using higher microwave power and for ^{23}Na, with its temperature-dependent T_{1e}, by performing experiments at lower temperatures. Sample considerations, such as sample volume, metal particle sizes, and dilution of metal particles, are also important for obtaining high enhancements. Studies of the hyperpolarization mechanism of the spins in diamagnetic environment at the interfaces between lithium metal and its passivating film suggest that both spin diffusion and direct chemical exchange play a role, although the role of direct cross-relaxation with the conduction electrons requires further investigation. The hyperpolarization is then transferred to spins farther from the metal surface via spin diffusion, allowing only the spins within less than ∼10 nm from the metal surface to be hyperpolarized. Based on the insights gained through this work, lithium metal possesses a possibly unique combination of beneficial qualities, making it a highly suitable system for Overhauser DNP. The high enhancements achieved for ^{6}Li (∼150) using a 1.3 mm rotor are particularly promising for studying lithium metal samples extracted from batteries, making use of the generally higher resolution of ^{6}Li over ^{7}Li.

DOI: 10.1103/tpch-2ftn

I. INTRODUCTION

More than 70 years ago (in *Physical Review*), the concept of nuclear hyperpolarization via electron spin saturation was predicted by Overhauser [1] and experimentally verified on lithium metal later that year by Carver and Slichter [2]: at a magnetic field strength of ∼3 mT and using a 50 W oscillator to irradiate the ESR transition of lithium metal, they achieved a nearly 100-fold enhancement of the ^{7}Li NMR signal. In our recent work, we demonstrated that nuclear hyperpolarization via an Overhauser mechanism could also be achieved on lithium metal at the much higher magnetic fields now available (9.4 T and 14.1 T for DNP/NMR spectroscopy) [3]. Moreover, it was shown that this method could be applied to hyperpolarize diamagnetic nuclei in the passivating film [or solid electrolyte interphase (SEI)] that forms on the surface of the lithium metal, making this a powerful technique to study many conductive solids and their surfaces or buried interfaces. More recent work by Leskes and coworkers has used Overhauser DNP to study the lithium metal dendrites that form in Li-conducting ceramic-polymer composites [4], while Zhang *et al.* used DNP at low fields to study lithium metal plating on carbon electrode materials [5].

In this work, we further investigate the Overhauser effect in alkali metals and explore some of the mechanisms in greater detail. Using a microstructural lithium sample packed in a 1.3 mm zirconia rotor, enhancements of close to 50 and 150 were obtained for ^{7}Li and ^{6}Li, respectively. For microstructural sodium metal, only a modest enhancement of 1.15 was obtained (in a 3.2 mm sapphire rotor). We start by briefly outlining the theory underpinning the Overhauser mechanism and the parameters that influence the signal enhancement, and then apply this theory to lithium and sodium metal to explain why

*Present address: Energy Storage and Distributed Resources Division, Lawrence Berkeley National Laboratory, 1 Cyclotron Road, Berkeley, California 94720, USA.

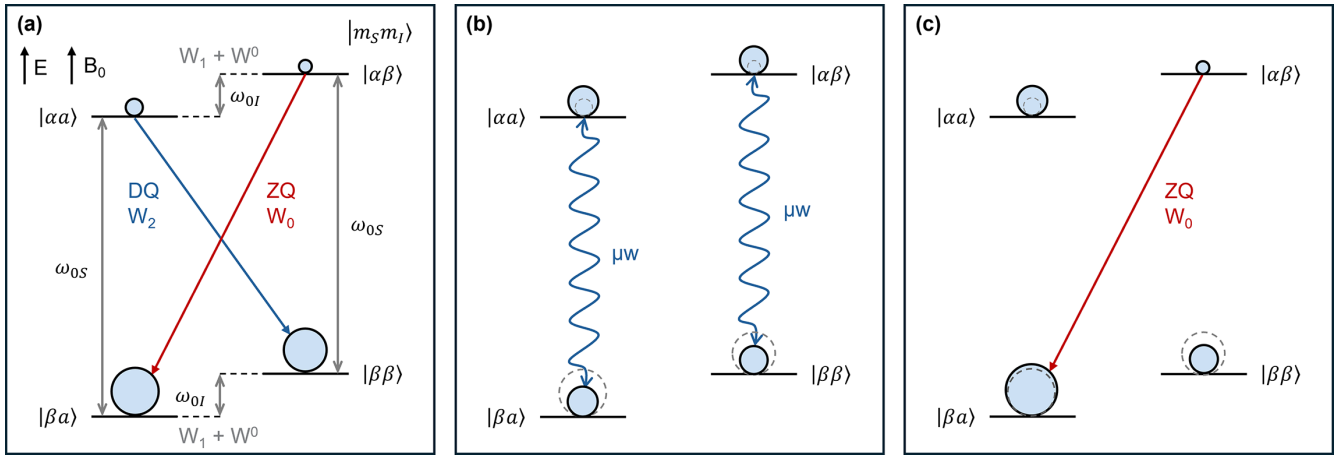

FIG. 1. (a) Schematic of the energy levels representing a coupled two-spin system, containing an electronic spin S and a nuclear spin I, in an applied magnetic field, B_0. The spin states are given by $|m_S, m_I\rangle$, where α and β represent up- and down-spin states, respectively. The splittings between the electron and nuclear spin states are denoted by their Larmor frequencies, ω_{0S} and ω_{0I}. The rates of nuclear transitions induced by the coupling with the electronic spin are given by W_0, W_1, and W_2, representing rates of the zero quantum (ZQ; red), single quantum (SQ; gray), and double quantum (DQ; blue) transitions, respectively. W^0 represents the rates of nuclear transitions arising from other mechanisms. The light blue circles represent the populations, which follow Boltzmann statistics under thermal equilibrium (a). (b) The electronic transitions induced by microwave irradiation, μw, are given by the blue wavy lines. During microwave irradiation, the spin populations are (partially) equalized. Dashed circles, which represent the initial populations, are drawn to illustrate schematically the difference in population. (c) Cross-relaxation of the electronic and nuclear spin via a ZQ transition, as is the case for lithium metal. The population difference between the nuclear spin states is now greater than under thermal equilibrium (as illustrated by the larger difference in area of circles depicting the magnetization of the α and β nuclear spins).

relatively modest enhancements are obtained. By systematically studying the ^{7}Li enhancements as a function of B_0 field, temperature, microwave power, and magic-angle spinning (MAS) frequency, coupled with spin-lattice (T_1) relaxation measurements, we verify that the nuclear relaxation of the metallic lithium spins (T_{1n}) is induced by cross-relaxation with the conduction electrons, and reveal that the experimental enhancements observed in our study are mostly limited by the degree of saturation of the electron spin magnetization. This is also true for ^{6}Li and ^{23}Na. Preliminary investigations on the hyperpolarization mechanism of the diamagnetic spins in and close to the metal-diamagnetic film interface suggest that the enhancement arises from both direct chemical exchange and spin diffusion; direct cross-relaxation with the conduction electrons, mediated via a scalar hyperfine interaction, is discussed, but definitive evidence for transfer via this mechanism requires further studies. The hyperpolarization is then transferred to spins farther from the metal surface via spin diffusion, allowing only the spins within a certain proximity to the metal to be hyperpolarized.

II. BACKGROUND

This section provides a brief description of the theory behind the Overhauser DNP mechanism. First, the relaxation process underpinning the Overhauser effect is discussed, followed by the requirements on the sample for this relaxation process to lead to hyperpolarization. Next, the parameters that govern the degree of hyperpolarization, and thus the enhancement of the NMR signal, are considered. Finally, the additional considerations when performing magnetic resonance experiments on metals are presented.

A. Overhauser effect

The Overhauser effect or "Overhauser DNP" relies on relaxation processes in which a coupled electron-nuclear spin pair is flipped simultaneously, where the relaxation processes are driven by time-dependent electron-nucleus ("hyperfine") interactions [1,6–8]. A qualitative description of the mechanism is as follows: consider an electronic spin S and a nuclear spin I in a static magnetic field B_0 that are coupled together via a hyperfine interaction, A. The four energy levels that represent this system and the transitions between the levels are shown in Fig. 1(a). The populations of these spin states are governed by Boltzmann statistics, where lower energy (spin) states are more populated than higher energy (spin) states. As result of the time dependences of the hyperfine interaction between the S and I spins (and thus fluctuating magnetic fields), there are relaxation processes in which the two spins flip simultaneously. The spins may flip in the same direction [the "double quantum" transition, DQ; $|\alpha\alpha\rangle \leftrightarrow |\beta\beta\rangle$] or in the opposite direction [the "zero quantum" transition, ZQ; $|\alpha\beta\rangle \leftrightarrow |\beta\alpha\rangle$]. The nature of the hyperfine coupling determines which of these transitions are allowed: fluctuations in the scalar interaction can induce only ZQ transitions, whereas the dipolar interaction may induce both ZQ and DQ transitions [6]. (The dipolar interaction also allows single quantum (SQ) transitions, in which only one of the spins flips, but this does not contribute to hyperpolarization of the I spins.) In an Overhauser DNP experiment, the system is irradiated at the electron Larmor frequency (ω_{0S}), inducing more electron spin flips from the lower to the higher energy spin states, as the lower spin state is originally more populated (following Boltzmann statistics), until the populations of the two spin states are equalized; this is known as saturation [Fig. 1(b)]. The system is now no longer in thermal equilibrium with

the lattice. As result, there are more relaxation transitions from the higher to the lower energy spin states (i.e., $|\alpha m_I\rangle \rightarrow |\beta m_I\rangle$) compared to those in the opposite direction. While most electron relaxation occurs via SQ pathways, and is thus independent of (i.e., decoupled from) the nuclear spins [6], the electronic spins can simultaneously "flip" the nuclear spins if relaxation occurs via a ZQ or DQ path. If the rate of ZQ and DQ relaxation differs, increased nuclear polarization (with a positive or negative sign), or "hyperpolarization," is generated [Fig. 1(c)].

To allow the simultaneous relaxation of the electronic and nuclear spins, two conditions must be met [6,7]: (1) the two spins are coupled, i.e., the Hamiltonian contains a term coupling the two spin states, and (2) fluctuations (spectral density) at the frequency (and thus energy difference) between these states must be present. The second condition can be explained as follows: the hyperfine interaction results in a magnetic field produced by the electron spins at the nucleus. Fluctuations in the hyperfine interaction may come from a time dependence in the coupling tensor, $A(t)$, or from time variations in $\boldsymbol{S}$, the electronic spin state. Various sources can give rise to the fluctuations: for liquids, a dipolar coupling may be modulated by internal dynamics (e.g., translational or rotational motion), whereas a scalar coupling can be modulated by very rapid relaxation of the electronic spin or rapid chemical exchange [7]. In the case of metals and semiconductors, the motion of the conduction electrons provides the time dependence of the coupling tensor.

In most nonmetallic solids containing paramagnetic centers, the S and I spins are in fixed positions, and thus no modulation of A generally occurs. For purely scalar coupling between the S and I spins (i.e., the nuclear and electronic spins belong to the same paramagnetic ion), an Overhauser effect should in theory be possible, if rapid electron spin flips (resulting in a reorientation of the electron spin magnetization, $\boldsymbol{S}$) of the appropriate frequency are present to provide the required fluctuations in the hyperfine interactions [6,7]. However, in general these nuclei are not readily observed due to the large hyperfine interactions (their resonance frequencies will be shifted and broadened). For a dipolar coupling in nonmetallic solids, the interaction predominantly induces SQ transitions and does not lead to nuclear hyperpolarization via an Overhauser effect; instead DNP via a solid effect may occur in systems with dilute paramagnetic centers [6]. The solid effect operates via a different mechanism and has been discussed in detail in review articles [6,9–12]. We note that DNP via an Overhauser mechanism has been observed in insulating solids, but the origin of the time-dependent hyperfine interaction responsible for driving the cross-relaxation remains unclear [12].

B. Rationalization of the signal enhancement in Overhauser DNP

The ratio of the nuclear polarization obtained via the Overhauser effect relative to that at thermal equilibrium is known as the DNP enhancement factor, ε, and can be evaluated from the expectation value of the nuclear magnetization, $\langle I_z\rangle$, in the coupled electron-nucleus system. From Fig. 1, the rate of change of the nuclear populations, and thus the nuclear polarization, can be written as [13]

$$\frac{d\langle I_z\rangle}{dt} = -(W_0 + 2W_1 + W_2 + W^0)(\langle I_z\rangle - I_0) - (W_2 - W_0)(\langle S_z\rangle - S_0), \tag{1}$$

where W_0, W_1, and W_2 are the rates of the ZQ, SQ, and DQ transitions induced by the electron spin S, and W^0 is the rate of nuclear SQ transitions induced via other mechanisms. $\langle S_z\rangle$ represents the expectation or time-averaged value of the electron magnetization, where $\langle I_z\rangle$ and $\langle S_z\rangle$ are given by I_0 and S_0 at thermal equilibrium. From Eq. (1), $\langle I_z\rangle$ at steady state ($\frac{d\langle I_z\rangle}{dt} = 0$) relative to I_0 is given by [6,8,14]

$$\frac{\langle I_z\rangle}{I_0} = 1 + \frac{W_2 - W_0}{W_0 + 2W_1 + W_2}\frac{W_0 + 2W_1 + W_2}{W_0 + 2W_1 + W_2 + W^0} \times \frac{(\langle S_z\rangle - S_0)}{S_0}\frac{S_0}{I_0}, \tag{2}$$

where the ratio $\frac{\langle I_z\rangle}{I_0}$ is the DNP enhancement factor, ε. The following definitions:

$$\xi = \frac{W_2 - W_0}{W_0 + 2W_1 + W_2}, \tag{3}$$

$$f = \frac{W_0 + 2W_1 + W_2}{W_0 + 2W_1 + W_2 + W^0}, \tag{4}$$

$$s = \frac{(S_0 - \langle S_z\rangle)}{S_0} \tag{5}$$

can then be used to rewrite Eq. (2) [6,8,14]:

$$\varepsilon = \frac{\langle I_z\rangle}{I_0} = 1 - \xi f s\frac{|\gamma_e|}{\gamma_n}, \tag{6}$$

where ξ, f, and s represent the coupling factor, leakage factor and saturation factor, respectively, and γ_e and γ_n are the gyromagnetic ratios of the electron and nuclear spins, respectively.

1. Coupling factor

The coupling factor (ξ) gives the difference between the DQ and ZQ relaxation rates (i.e., the transitions that result in hyperpolarization), relative to the sum of the rates for all nuclear spin transitions induced by the coupling to the electron spin. The coupling factor, thus, reflects the relative contributions of the time-dependent components of the hyperfine interaction, namely, the scalar and dipolar hyperfine terms. In the case of a purely scalar interaction, the rate of the electron-induced nuclear SQ and electron-nuclear DQ transitions are zero (i.e., $W_1 = W_2 = 0$), and thus the coupling factor, to a first approximation, is equal to -1. For a purely dipolar interaction in the extreme narrowing limit (where $W_0 : W_1 : W_2 = 2 : 3 : 12$), the coupling factor is equal to 0.5 [6,15]. As expressions for W_1 and W_2 depend on the electronic and nuclear Larmor frequencies (ω_S and ω_I) and the correlation time of the motion inducing the relaxation (τ_c), the coupling factor for a dipolar interaction shows a strong dependence on the field strength B_0 and temperature (provided that the motion is temperature dependent) [8,13].

More specifically, Overhauser DNP based on a dipolar hyperfine interaction becomes less efficient at higher field strengths and for longer correlation times [8,16]. For a purely

scalar interaction, where the fluctuations in the hyperfine interaction arise through a modulation in the coupling tensor, $A(t)$ (due to, e.g., motion of the electrons/atoms and/or chemical exchange, referred to by Abragam as scalar relaxation of the first kind [7]), $\xi = \frac{-W_0}{W_0} = -1$, canceling out any temperature and field dependencies. This is the case for lithium metal (and other alkali metals) [17]. If the scalar hyperfine interaction is modulated by rapid reorientation of the electron spin, S (scalar relaxation of the second kind [7]), the relaxation rate W_1 is no longer zero, and $\xi < -1$ [7]. This relaxation mechanism is distinct from mechanisms that involve any time dependence of A and may involve the large fluctuations driven by magnetic interactions between spins (e.g., involving dipolar, exchange interactions, and spin-orbit coupling mechanisms), and S is now time dependent, $S(t)$. In solids with rapid mobility of the ions and the electrons, multiple terms may need to be considered. For example, in a system undergoing spin exchange (e.g., when an unpaired electron hops between neighboring molecules or atoms) the relative contribution of this motional process to the relaxation processes will depend on the lifetime of the electron-nucleus complex τ_c. If τ_c is longer than the electron relaxation times (T_{1e} and T_{2e}), the effect of $S(t)$ is "felt." In this scenario, the deviation of coupling factor from -1 depends on the field strength B_0 (and temperature, via changes in τ_c) and ξ tends to zero for $\omega_S \tau_c \gg 1$, i.e., W_1 dominates [8,13].

2. Leakage factor

The leakage factor (f) describes the fraction of nuclear relaxation that is caused by the coupling to the electron spin, relative to that induced via all possible relaxation mechanisms. For $f = 1$, nuclear relaxation arises exclusively from the mechanisms driven by the electron spins (i.e., $(T_{1n})_e, = (T_{1n})_{\text{total}}$), whereas for $f = 0$, none of the nuclear relaxation is caused by the electron spin.

The leakage factor may be expressed as a ratio of the nuclear relaxation time constants, $(T_{1n})_{\text{total}}$ and $(T_{1n})_e$, by rewriting Eq. (4) as [6]

$$f = \frac{W_0 + 2W_1 + W_2}{W_0 + 2W_1 + W_2 + W^0} = \frac{(R_{1n})_e}{(R_{1n})_{\text{total}}} = \frac{(T_{1n})_{\text{total}}}{(T_{1n})_e}, \quad (7)$$

where $(R_{1n})_e$ and $(R_{1n})_{\text{total}}$ represent the electron-induced and the total rates of nuclear relaxation, respectively. If the relaxation time constants can be measured, the leakage factor may be determined experimentally (e.g., for liquids with and without the presence of the radical source [18]). Note that this is more challenging (if not impossible) for solids.

3. Saturation factor

The saturation factor (s) describes the degree to which the populations of the electronic spins states are equalized as a result of microwave irradiation. Here s can range from 0 to 1, where for $s = 1$, the two populations are fully equalized, and for $s = 0$, the populations are those at thermal equilibrium. An intermediate value of s indicates partial equalization of the populations.

The degree of saturation of the electron transition is governed by the interplay between microwave irradiation and electron relaxation. The microwave irradiation at the electron frequency induces transitions in both directions, equalizing the populations, whereas the interaction between the spins and the lattice tries to establish a (thermal) equilibrium distribution of the spins over the two energy levels. The expectation value $\langle S_z \rangle$ is given by [8]

$$\frac{d\langle S_z \rangle}{dt} = \frac{1}{T_{1e}}(\langle S_z \rangle - S_0) - \gamma_e^2 B_{1,e}^2 T_{2e} \langle S_z \rangle, \quad (8)$$

where T_{1e} and T_{2e} are the electronic spin-lattice and spin-spin relaxation time constants, respectively, and $B_{1,e}$ is the field strength of the microwave irradiation. Equation (8) can be solved under steady-state conditions ($\frac{d\langle S_z \rangle}{dt} = 0$), and the saturation factor in Eq. (5) may be written as [1,8,19]

$$s = \frac{(S_0 - \langle S_z \rangle)}{S_0} = \frac{\gamma_e^2 B_{1,e}^2 T_{1e} T_{2e}}{1 + \gamma_e^2 B_{1,e}^2 T_{1e} T_{2e}}. \quad (9)$$

The amplitude of the applied microwave field strength squared, $B_{1,e}^2$, is proportional to the microwave power (W), and thus the degree of saturation depends on the electronic relaxation times, T_{1e} and T_{2e}, and the applied microwave power experienced by the spins.

In summary, to achieve the theoretical maximum enhancement as determined by the ratio of the electron and nuclear gyromagnetic ratio [Eq. (6)], the coupling, leakage, and saturation factors all must be (close to) $(-)1$. This means that the electron-nuclear coupling has to be purely scalar ($\xi = -1$), all nuclear relaxation induced by the electron spins ($f = 1$), and the electron transitions should be fully saturated ($s = 1$), in practice requiring high microwave power ($B_{1,e}^2$) and long electron relaxation times (T_{1e} and T_{2e}).

C. Magnetic resonance of metals

When performing magnetic resonance experiments (both NMR and ESR) on metals, additional phenomena need to be considered. Since the conduction electrons are delocalized, each nuclear spin simultaneously interacts with all the conduction electrons in the sample. This is different from solids containing paramagnetic ions, where the electron is localized on the atom or ion it belongs to and the nuclear spins "see" a time average of the localized electron spins [6,20]. Intermediate systems exist, for example, in half metals, where both delocalized bands and localized spins are present. The presence of the delocalized conduction electrons affects the radiofrequency (r.f.) and microwave fields entering the metal sample, the shift of the nuclear resonance, and nuclear relaxation. Below we discuss these phenomena, all of which are relevant to lithium metal Overhauser DNP.

1. Skin effect

Electromagnetic radiation, such as microwave and radiofrequency radiation, is rapidly attenuated upon entering a metal (or any conductor) and decays exponentially over a characteristic distance δ, known as the skin depth [20],

$$\delta = \sqrt{\frac{\rho}{\pi \mu_0 \mu_r \nu}}, \quad (10)$$

where ρ is the electrical resistivity of the metal, μ_0 is the vacuum permeability, μ_r is the relative permeability of the

metal, and ν is the frequency of the radiation in Hertz. The skin depth is reduced at lower temperatures, due to a lower electrical resistivity, and for higher frequencies of radiation. For the present work performed on lithium metal using a B_0 field of 9.4 T, the radiofrequency skin depth for ^{7}Li experiments (∼156 MHz) is ∼10 μm at 300 K and ∼3.4 μm at 100 K, while the microwave skin depth for electron irradiation (∼264 GHz) is ∼0.25 μm at 300 K and ∼0.08 μm at 100 K [21].

Both NMR and ESR measurements on metal particles may be affected by skin effects. In NMR experiments, the skin effect may prevent one from probing all lithium spins in lithium metal if the particles are larger than the skin depth. In this case, nutation curves will appear distorted and attenuated, meaning that a simple nutation experiment is an effective method to verify whether the NMR experiment is affected by skin effects. Nutation experiments on a representative microstructural lithium sample are shown in the Supplemental Material (SM; see note S1 [22]).

In conduction ESR (CESR) experiments, skin effects may similarly prevent all electrons from contributing to the ESR signal. However, this case is more complicated since the conduction electrons near the Fermi level rapidly diffuse across the whole particle, resulting in two main consequences. First, the CESR line shape in continuous wave (CW) ESR appears asymmetric—a so-called Dysonian line—with the exact shape depending on the ratio of skin depth and particle thickness [23]. Regarding the electronic relaxation times, the spin-spin interactions are negligible in alkali metals, and therefore $T_{1e} = T_{2e}$ in (alkali) metals [24]. Both relaxation time constants are therefore normally determined from the CESR linewidth (especially in older literature).

Second, an electron spin that has been irradiated at the surface can travel a certain distance before it undergoes a spin flip, the magnetization returning to equilibrium. This average distance is known as the spin depth, δ_e, and is given by [25]

$$\delta_e = \sqrt{2DT_{2e}}, \tag{11}$$

where D is the electron diffusivity and T_{2e} is the average time over which the electron maintains its saturation (its relaxation time constant). If the *spin* depth is greater than the *skin* depth, electrons within the skin depth that have been irradiated can travel in and out of the bulk, maintaining transverse magnetization, while those originally in the bulk can move into the spin depth region, where they are then irradiated and thus contribute to the CESR signal. For lithium metal at room temperature, $T_{2e} = \sim 200$ ns [24] and $D = 21\,\mathrm{cm^2\,s^{-1}}$ [26], yielding a spin depth of ∼29 μm. This implies that in an Overhauser DNP experiment on lithium metal, the nuclear hyperpolarization originating from electron-nuclear cross-relaxation with saturated electron spins can occur farther inside the metal particle than the skin depth would suggest, due to this electron spin diffusion. Moreover, it has been proposed that the electron spin saturation will be uniform within the metal particle (with dimensions d), but is reduced by a factor on the order of (δ_e/d) resulting in a spread of the observed electron and nuclear frequencies [27].

Comparing the room temperature spin depth for lithium metal to the average diameter of the individual lithium metal particles (1–5 μm) used in this work [3] [see Fig. S2 for representative scanning electron microscopy (SEM) images [22]], the saturation level of the electron spins is expected to be uniform within each metal particle for experiments performed at room temperature. This latter statement assumes that the dendrites are well separated from each other and that the microwave power can uniformly enter the sample or dendrite—an assumption that is explored below.

2. *Frequency shift in metals: The Knight shift*

The nuclear resonance of spins in a metal has a characteristic shift, the so-called Knight shift, which moves its position away from where it would appear in a nonmetallic environment. The coupling between the unpaired electron spin density and the nuclear spins results in an additional magnetic field experienced by the nuclear spins, B_e, which results in a positive frequency shift K, the Knight shift [6,28,29],

$$K = \frac{B_e}{B_0} = \frac{8\pi}{3}\langle|\psi_s(0)|^2\rangle_F \chi_p, \tag{12}$$

where $\langle|\psi_s(0)|^2\rangle_F$ is the square of the s wave function at the nucleus, averaged over the electrons at the Fermi level and χ_p is the paramagnetic susceptibility per unit volume. As the unpaired electron spin density is essentially temperature independent (typically referred to as the temperature-independent Pauli susceptibility), the Knight shift shows no or a weak temperature dependence in most cases. The Knight shift is reduced by microwave irradiation of the CESR transition, as this decreases the net electron spin magnetization and thus the paramagnetic susceptibility (see note S3 for a more detailed explanation [22]) [2,3].

3. *Nuclear relaxation in metals: The Korringa relationship*

In metals three main mechanisms contribute to the longitudinal relaxation of the nuclear spins: the hyperfine interaction between the nuclear spins and the conduction electrons [leading to Overhauser (OE) hyperpolarization], the magnetic dipolar interaction between neighboring nuclei, and the electric quadrupolar coupling of the nuclear quadrupole moments and the local electric field [30]. The quadrupolar mechanism is negligible in metallic lithium (and all metals with cubic symmetry) [30–32].

Out of these three mechanisms, the coupling between the nuclear spins and the conduction electrons is unique to metals. The temperature dependence of $(T_{1n})_e$ in a metal is described by the Korringa relationship and is inversely proportional to the absolute temperature [33]:

$$(T_{1n})_e K^2 = \frac{\hbar}{4\pi k_B T}\left(\frac{\gamma_e}{\gamma_n}\right)^2, \tag{13}$$

where $\hbar$ is the reduced Planck constant, and k_B is the Boltzmann constant. For metallic lithium this equation is equal to $(T_{1n})_e = 43.4/T$. The Korringa relation holds for the experimentally measured T_{1n} if the nuclear relaxation is primarily caused by cross-relaxation with the conduction electrons.

Finally, a practical limitation in MAS NMR of metals is the ability to spin conductive samples, the eddy currents producing magnetic fields that oppose the rotation. To avoid this, metallic samples are generally heavily diluted with a nonconducting, inert solid such as KBr or silica.

4. Electronic relaxation in metals

Relaxation of the electronic spin in alkali metals occurs due to the combined effects of collisions of the conduction electrons with lattice vibrations (phonons) and lattice imperfections and spin-orbit coupling [19,20,24,34]. The spin-orbit interaction causes slight mixing of the spin states, and as a result, a collision can lead to the reorientation of the electronic spin with probability Δg^2, where Δg represents the deviation of the electronic g value from that of a free electron, larger values of Δg reflecting larger spin-orbit coupling (and orbital angular momentum). The electronic relaxation time constant depends on collision rate (i.e., quantified via the inverse of the electrical resistivity relaxation time constant, T_R), divided by Δg^2 [34]:

$$T_e \sim \frac{T_R}{(\Delta g)^2}. \tag{14}$$

The collision rate, T_R^{-1}, can be divided into contributions from collisions with lattice vibrations, T_p^{-1}, and with lattice imperfections, T_l^{-1} [20,34]:

$$\frac{1}{T_R} = \frac{1}{T_p} + \frac{1}{T_l}. \tag{15}$$

The rate of collisions with lattice vibrations is strongly dependent on temperature, while the rate of collisions with imperfections depends on the purity of the metal and is essentially temperature independent.

Lithium metal, with its small spin-orbit coupling and negligibly small value of Δg, exhibits relatively long electronic relaxation times compared to other alkali metals, with the relaxation mechanism dominated by impurity scattering. The intrinsic T_{1e} and T_{2e} of lithium metal are thus essentially temperature independent, and instead scale with the purity of the sample: Feher and Kip measured a T_{2e} of $\sim 3 \times 10^{-9}$ s for 99% pure lithium, which increases to $\sim 2.5 \times 10^{-8}$ s for 99.9% purity ($T_{1e} = T_{2e}$ for alkali metals; see Sec. II C 1) [24]. For sodium with its larger value of Δg, the electronic relaxation time is now temperature dependent, the T_{2e} increasing from $\sim 1 \times 10^{-8}$ s at 300 K, to $\sim 3.5 \times 10^{-8}$ s at 80 K, and $\sim 1 \times 10^{-7}$ s at 20 K [24,35,36].

III. EXPERIMENTAL

A. Sample preparation

Microstructural lithium samples were obtained by plating lithium on lithium foil disks: lithium foil disks (lithium metal foil; 99%, Aldrich, and 99.95%, LTS Research) were used as received. A series of different electrolyte solutions were used, as part of ongoing studies to explore the effect of electrolyte on dendrite formation. The first electrolyte comprised 1 M $LiPF_6$ in ethylene carbonate and dimethyl carbonate (EC:DMC, 1:1 v/v, battery grade, Sigma-Aldrich, termed "LP30"). The second electrolyte comprised 1 M $LiPF_6$ in ethylene carbonate and dimethyl carbonate (EC:EMC, 3:7 v/v, battery grade, Sigma-Aldrich, termed "LP57"). The third electrolyte comprised 1 M LiTFSI in tetraglyme (Sigma-Aldrich); this electrolyte was used to prepare samples described in the SM Fig. S4 [22]. Microstructural sodium samples were prepared analogously, by plating sodium on sodium foil disks (sodium cubes in mineral oil, 99.9% trace metal basis, Sigma) using a 1 M $NaPF_6$ in PC (Sigma-Aldrich) electrolyte.

Li-Li and Na-Na cells were assembled in a coin cell configuration: a stainless-steel spacer (0.5 mm thick), a lithium or sodium metal disk, a polypropylene-polyethylene separator (Celgard 3501, rinsed with ethanol and dried under dynamic vacuum at 40 °C for 24 hours) wetted with 75 μL of electrolyte solution, a second lithium or sodium metal disk, a stainless-steel spacer (0.5 mm thick), and a stainless-steel conical spring were compressed in a 2032-type coin cell casing. All cell assembly was performed in an argon-filled glovebox (MBraun, O_2 and $H_2O < 1$ ppm).

A typical procedure is as follows (with deviations noted where relevant in the text): galvanostatic electrodeposition was performed using a Biologic MPG2 potentiostat/galvanostat instrument running EC-lab software. A constant current of 1.25 mA cm^{-2} was applied in a single direction for 3 hours and 12 min, for a capacity of 4 mAh cm^{-2}.

The coin cells were disassembled in an argon-filled glovebox, and the plated microstructural lithium or sodium metal was dried under dynamic vacuum for 10–30 minutes, without rinsing the metal foil. The microstructural lithium or sodium metal was scraped off gently with a spatula. The metal sample was then diluted with KBr (dried under dynamic vacuum at 200 °C for 48 hours; Li : Li = 1:20 by mass, Na : Na = 1:10) by lightly hand grinding the mixture in a mortar and pestle, to improve microwave penetration and allow the metallic samples to be more easily spun. The lithium metal sample was packed into a 3.2 mm outer diameter sapphire magic-angle spinning (MAS) rotor (containing ~2 mg lithium metal) or a 1.3 mm outer diameter zirconia MAS rotor (~0.2 mg lithium metal). The sodium sample was packed into a 3.2 mm sapphire MAS rotor (~5 mg sodium metal). To protect the metallic samples from exposure to air, a thin layer of KBr was added on top of the metallic sample, followed by a layer of polytetrafluoroethylene (PTFE) tape. Additionally, PTFE tape was applied around the stem of the rotor cap before placing it into the rotor, improving the rotor seal. The rotors were stored in an argon-filled glovebox when they were not used for NMR experiments.

The sample used for recording SEM images was a Li-Li assembled coin cell, configured as described above, utilizing LP57 electrolyte. Galvanostatic electrodeposition was performed at a constant current of 0.5 mA cm^{-2} in a single direction for 1 hour, achieving a capacity of 1 mAh cm^{-2}. The coin cell was disassembled in an argon-filled glovebox, and the plated lithium anode with microstructural lithium metal was dried under dynamic vacuum for 10 minutes. A quarter of the lithium anode was cut and directly mounted in the SEM module, while the remaining lithium anode was gently scraped using a spatula to extract the microstructure. Half of the scraped lithium microstructure was also mounted in the SEM module, and the other half was mixed and ground

with KBr (Li : Li = 1:5 by mass) before being mounted in the SEM module.

B. DNP-enhanced solid-state NMR spectroscopy

Solid-state ^{7}Li and ^{6}Li magic-angle spinning (MAS) NMR experiments were performed on a Bruker 9.4 T Avance Neo spectrometer with a 264.2 GHz klystron microwave source (Bruker) [37], using 3.2 mm and 1.3 mm wide-bore Bruker DNP probes. ^{23}Na and additional ^{7}Li MAS NMR experiments were performed on a 14.1 T Bruker AVANCE III HD spectrometer with a 395 GHz gyrotron microwave source (Bruker), using a 3.2 mm wide-bore DNP probe. The B_0 field of both magnets could be varied by a few tens of mT, by using a superconducting sweep coil. Variable-temperature measurements between ∼100 and ∼250 K were performed using a Bruker LTMAS cabinet, while room temperature experiments were performed with RT nitrogen gas. The klystron microwave power is reported as the nominal power produced at the klystron microwave source, with set values between 0.5 and 5.2 W.

For the ^{7}Li and ^{79}Br NMR experiments performed at 9.4 T on the 3.2 mm DNP probe, radiofrequency (r.f.) field strengths of 56 kHz for ^{7}Li and 66 kHz for ^{79}Br at room temperature, and 66 kHz for ^{7}Li at ∼95 K were used. Quantitative recycle delays ($5 \times T_1$) were used for the ^{7}Li NMR spectra: 0.8 s and 2.3 s for the metal signal at room temperature and ∼95 K, respectively. Recycle delays of 10 s were used for the ^{7}Li diamagnetic signal at room temperature. For the ^{7}Li and ^{23}Na NMR experiments performed at 14.1 T, the r.f. field strengths were 45 kHz for ^{7}Li and 55 kHz for ^{23}Na, with recycle delays of 1 s. One-dimensional spectra were acquired using either a one-pulse excitation or a Hahn echo pulse sequence. Two-dimensional exchange correlation spectroscopy (EXSY) spectra were acquired with a mixing times of 50 ms to 1 s. All pulse sequences included a presaturation sequence. Longitudinal nuclear relaxation times, T_{1n}, were measured using a saturation-recovery pulse sequence.

Due to the narrow ESR linewidth of lithium metal and the frequency instability of the microwave sources (see Sec. V D), the B_0 field was optimized prior to every experiment. The magnetic field position was set to maximum enhancement using first the superconducting sweep coil of our DNP-NMR magnet for rough adjustment (not always necessary) and then optimized using the lock field of the Bruker Smart Magnet control System (BSMS, "Field" value). For fine adjustment, the lock field value was typically varied in steps of 200, corresponding to ∼2.34 ppm. No frequency lock was applied. AU programs for setting the lock field from the Topspin command line and for sweeping through a number of lock field values are provided in the SM (see note S4 [22]).

^{7}Li NMR spectra were externally referenced to LiF at −1 ppm at room temperature. ^{23}Na NMR spectra were referenced internally to the diamagnetic signal at 0 ppm. DNP enhancement factors, ε, were calculated as the ratio of the integrated signal intensities of spectra acquired with and without microwave irradiation ($\varepsilon = A_{on}/A_{off}$). The sample temperature was determined from the ^{79}Br chemical shift and T_1 of KBr [38] for measurements at room temperature and ∼100 K, respectively.

C. ESR spectroscopy

CW ESR spectroscopy of lithium metal dendrites was carried out on a benchtop X-band ESR spectrometer (MS5000, Magnettech) at a microwave frequency of 9.437 GHz. A microwave power of 0.6 mW was used and the magnetic field was modulated at a frequency of 100 kHz and an amplitude of 0.001 mT. The ESR measurement was performed at room temperature on the same 3.2 mm rotor packed with lithium dendrites that was used for the DNP experiments. The rotor was placed in an ESR sample tube and positioned in the center of the ESR cavity.

IV. RESULTS

To explore the Overhauser mechanism in lithium metal, a microstructural lithium sample was prepared in a similar manner as described in Ref. [3]: lithium microstructures were grown electrochemically in a lithium-lithium electrochemical cell, extracted and diluted with KBr, before being packed in 3.2 and 1.3 mm MAS rotors. SEM images of the as-prepared lithium dendrites show two typical dendrite morphologies, one "thin" with filaments approximately 1 μm in size, and one thicker comprising branches that are >2 μm in diameter but forming clumps that are 5–10 μm in diameter; it is, however, difficult to obtain clear images of the dendrites after grinding with KBr (Fig. S2 [22]). ^{7}Li nutation experiments on a variety of the KBr-packed lithium dendrite samples typically demonstrate a sine curve for the NMR signal as a function of the flip angle (Fig. S1 [22]). This indicates that the NMR measurements of KBr diluted samples are generally not affected by NMR skin effects, which is consistent with the individual lithium dendrite filaments or branches being smaller or of the same order of magnitude as the ^{7}Li radio frequency NMR skin depth (∼10 μm and ∼3.4 μm at 300 K and 100 K, respectively for a ^{7}Li NMR pulse at a frequency of 156 MHz).

A. Metallic lithium signal

The room temperature ^{7}Li MAS NMR spectra of microstructural lithium metal with and without microwave irradiation are shown in Fig. 2 for a 3.2 mm sapphire rotor [Fig. 2(a)] and a 1.3 mm zirconia rotor [Fig. 2(b)]. The appearance of the spectra and the effects of microwave irradiation correspond to what has been discussed in our previous work [3]: the ^{7}Li NMR spectra show two signals; the main signal at ∼260 ppm arises from the metallic spins, where the large shift (Knight) is due to the scalar hyperfine interaction between the nuclear spins and the conduction electrons [28]. The signal at ∼0 ppm arises from lithium salts on the surface of the metal, coming from the SEI and residual electrolyte salt [3]. These salts include inorganic and organic salts such as LiF, Li_2CO_3, and lithium ethylene decarbonate (LEDC), which form as a result of the reduction of the solvent and attack of the electrolyte salt ($LiPF_6$) by the resulting degradation products on or close to the surface of lithium metal. This signal will be referred to as the "diamagnetic" lithium signal. Upon microwave irradiation, two observations can be made concerning the metal signal: first, a noticeable enhancement is obtained (∼13 for 3.2 mm rotor, and ∼56 for 1.3 mm rotor); second, microwave irradiation results in a spreading

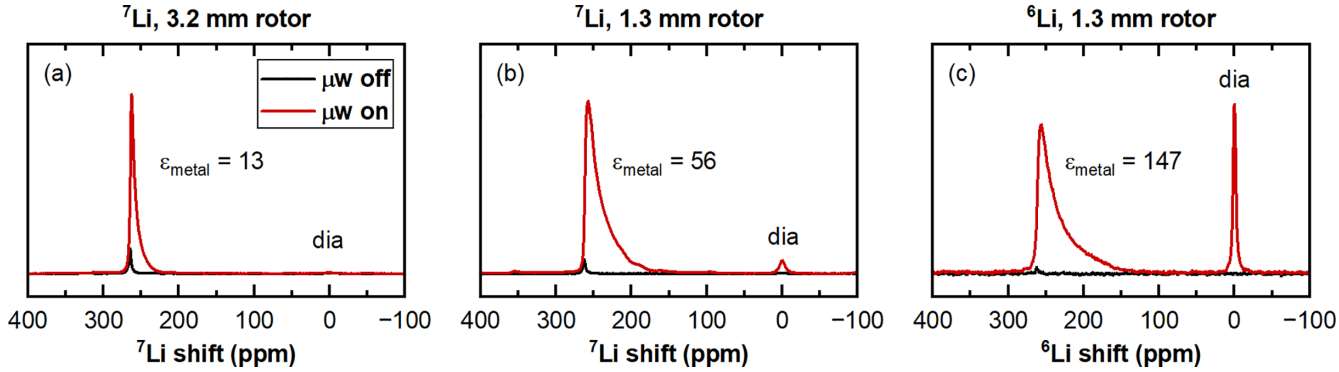

FIG. 2. ^{7}Li - ^{6}Li NMR spectra of microstructural lithium metal without (black) and with (red) 5.2 W of microwave (μw) irradiation at 264.2 GHz, recorded at 9.4 T and a sample temperature of ∼300 K: (a) ^{7}Li NMR spectra acquired in a 3.2 mm sapphire rotor at 8 kHz MAS, (b) ^{7}Li NMR spectra acquired in a 1.3 mm zirconia rotor at 15 kHz MAS and (c) ^{6}Li NMR spectra acquired in a 1.3 mm zirconia rotor at 25 kHz MAS. The signal at 264 ppm arises from the metallic lithium spins and the signal at 0 ppm (labeled "dia") is ascribed to lithium salts on the surface of lithium metal. Note that all spectra are of the same sample, packed in either a 3.2 or a 1.3 mm rotor.

of the lithium metal signal to lower frequencies: the Knight shift is reduced by ∼1 − 1.5 ppm (for 3.2 mm rotor) and over ∼6 ppm (for the 1.3 mm rotor) as determined by the shift of the signal maximum.

The ∼4.3× greater enhancements obtained with a 1.3 mm rotor are mostly attributed to the improved microwave wave guide coupling on the 1.3 mm probe [39] as well as the smaller sample volume of the rotor and thus greater microwave penetration into the sample. Even though the microwave irradiation is expected to be uniform for all spins within one particle (due to the rapid mobility of the conduction electrons and large spin depth; see Sec. II C 1) [3], the collection of often agglomerated individual metal particles can still rapidly attenuate the microwave field as it enters the metal/KBr-filled rotor (1:10 lithium metal to KBr dilution), limiting the microwave penetration deeper into the rotor. The higher surface-to-volume ratio for the 1.3 mm rotor may allow for a larger fraction of the sample to be irradiated with higher microwave power, leading to higher enhancements.

The Knight shift reduction is more pronounced for the 1.3 mm rotor (>5 ppm), again indicating a greater degree of saturation of the electronic spins compared to the 3.2 mm rotor, which is consistent with the 1.3 mm rotor allowing for more effective microwave irradiation of the sample and the higher enhancement in this case [39].

Due to the metallic lithium NMR signal spreading to lower frequencies upon microwave irradiation, different enhancement values are calculated when considering the change in peak height ($\varepsilon_{intensity}$) or area ($\varepsilon_{integral}$ or ε). Integrating the full signal ($\varepsilon_{integral}$) provides a more accurate insight into the degree of hyperpolarization of the ensemble of metallic spins; however, $\varepsilon_{intensity}$ may be relevant in cases where the signal-to-noise ratio is more important. All enhancements reported above and in the rest of this work are given as $\varepsilon_{integral}$, as this allows for a better analysis of the hyperpolarization mechanism and a more direct comparison between the enhancements obtained from the metal and diamagnetic signals.

For B_0 field optimizations both $\varepsilon_{intensity}$ and $\varepsilon_{integral}$ can be used, but $\varepsilon_{intensity}$ may be preferred, as it can be evaluated by simple visual comparison and can then be used to calculate (or experimentally determine) the optimal field for $\varepsilon_{integral}$. The B_0 field at which the maximum enhancement is observed for $\varepsilon_{intensity}$ and $\varepsilon_{integral}$ differ slightly: the optimal field for $\varepsilon_{intensity}$ is consistently ∼2.3 ppm (≙360 Hz ≙0.02 mT for $B_0 = 9.4$ T), lower than that for $\varepsilon_{integral}$ for the lithium metal samples and DNP setup used in this work.

Figure 2(c) shows the room temperature ^{6}Li NMR spectra with and without microwave irradiation recorded on the same 1.3 mm rotor: an enhancement of ∼147 was obtained for the metal signal. The higher ^{6}Li enhancement is due to the lower gyromagnetic ratio of ^{6}Li [Eq. (6)], and the increase in enhancement for the ^{6}Li signal compared to that of ^{7}Li [$\varepsilon(^6\text{Li})/\varepsilon(^7\text{Li})2.62$] is approximately equal to the ratio of the two gyromagnetic ratios $\frac{\gamma_{^7Li}}{\gamma_{^6Li}} = 2.64$. Such high enhancements enable the acquisition of ^{6}Li NMR spectra on small quantities of lithium metal (∼0.2 mg) at natural abundance within minutes, which would not be possible without DNP. This may prove very beneficial for investigations of the lithium metal surface/interface, due to the higher spectral resolution in the diamagnetic region of ^{6}Li NMR spectra compared to ^{7}Li [40].

1. Enhancement vs applied magnetic field strength (B_0)

The field profile of the enhancement of the metallic signal [Fig. 3(a)] shows a positive enhancement. As we have shown before [41], this corresponds to the metal signal being enhanced via an Overhauser mechanism where the rate of zero-quantum (ZQ) cross-relaxation is greater than that of the double-quantum (DQ) cross-relaxation, given that the gyromagnetic ratio of ^{7}Li is positive and that of an electron is negative. Similar to our previous work on the metallic signal [3], no evidence for a solid-effect DNP mechanism could be detected, which would occur at magnetic fields of ±5.6 mT from the CESR resonance at 9.4 T.

The field profile of the nuclear enhancement measured at 9.4 T also tracks the X-band ESR absorption signal of lithium metal acquired on the same rotor (Fig. 3; see Fig. S4 for ESR spectra [22]). No significant broadening of the CESR line (in mT) occurs at high fields, consistent with the symmetric environment for lithium and lack of g-anisotropy, in addition to the rapid mobility of the electrons [20]. Therefore, the B_0 field range for achieving enhancements in lithium metal DNP

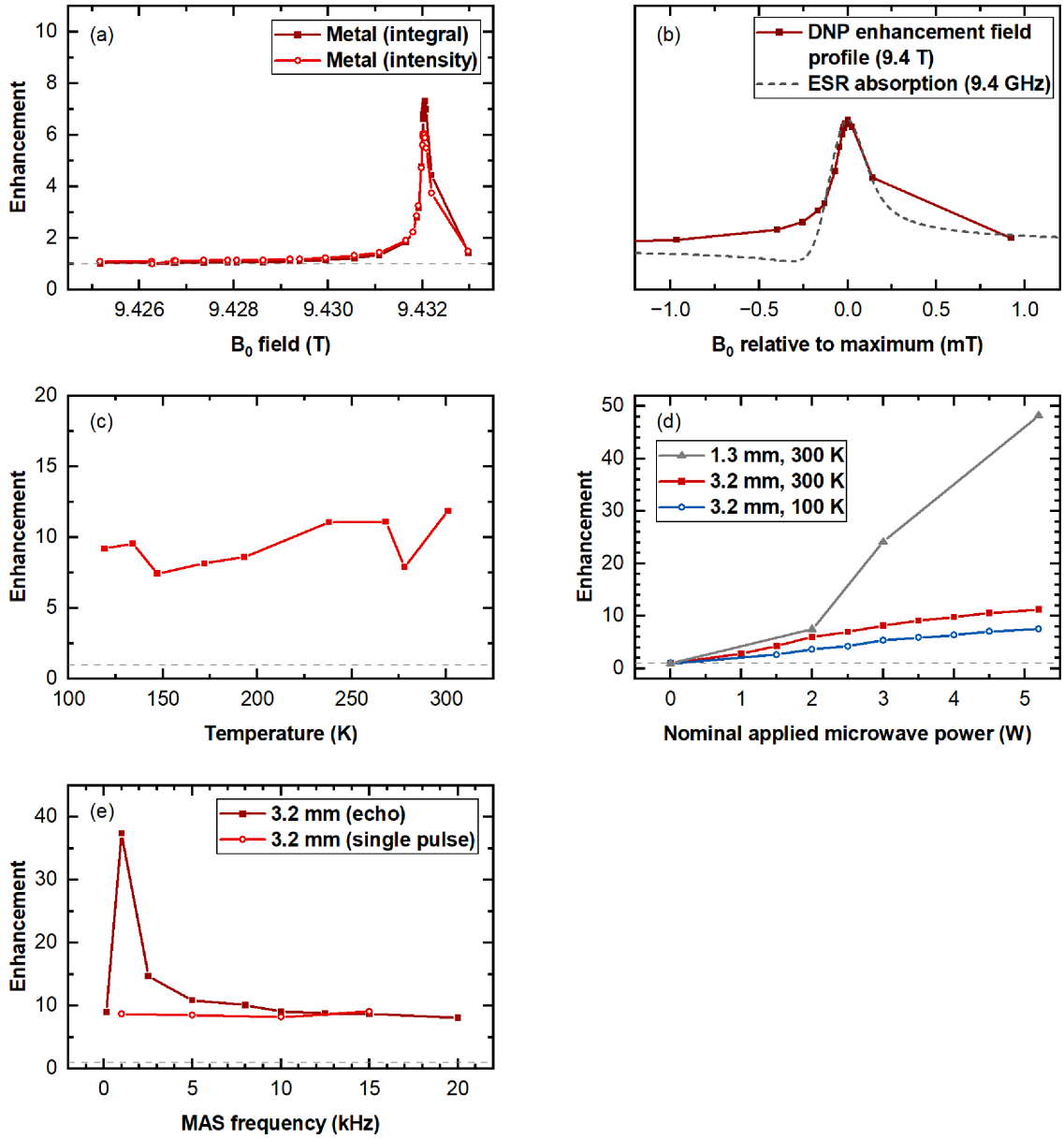

FIG. 3. Enhancement of the metallic ^{7}Li NMR signal of microstructural lithium metal as a function of the applied magnetic field strength, B_0, (a) and (b) a comparison of lithium CESR lineshape with the field profile shown in (a). Enhancement of the metallic ^{7}Li NMR signal as a function of (c) temperature, (d) nominal applied microwave power, and (e) MAS frequency. The B_0 field was optimized prior to measuring each data point in (c)–(e). The gray dashed horizontal line represents no enhancement ($\varepsilon = 1$). The data points are connected to guide the eye. The enhancement is obtained by integrating the lithium metal signal.

is very narrow, particularly in comparison with bisnitroxide radicals. The consequences of this on the DNP experiments will be discussed in Sec. V D.

2. Enhancement vs temperature

The enhancement of the metallic lithium signal shows no strong temperature dependence [Fig. 3(c)]: the enhancement fluctuates between 8 and 12 over the temperature range 100–300 K. Marginally higher enhancements were often observed at room temperature compared to low temperatures (∼100 K). This is clearly seen in Fig. 3(d), where the room temperature enhancements (red) are consistently higher. However, it is important to stress that the extremely narrow CESR linewidth, coupled with the instability of our klystron means that some of this variability is associated with small drifts of the klystron frequency (see below).

3. Enhancement vs microwave power

The enhancement of the metallic lithium signal as a function of the nominal applied microwave power, using the klystron, at 300 K (for 3.2 mm rotor; red, and 1.3 mm rotor; gray) and 95 K (for 3.2 mm rotor only; blue) is shown in Fig. 3(d). As expected, the enhancement increases for higher microwave powers, which is ascribed to a higher degree of electron spin saturation [Eq. (9)]. Even though the exact microwave field at the sample is not known, the enhancement

increases almost linearly with increasing microwave power and has not yet plateaued at 5.2 W klystron power, indicating that significant levels of saturation have not been achieved. This is also consistent with the only small reduction of the Knight shift.

4. Enhancement vs MAS frequency

The influence of the MAS frequency on the enhancement of the metallic signal at room temperature is shown in Fig. 3(e). The enhancement of the metallic signal shows no dependence on the MAS frequency and is also comparable under static conditions. This is promising for *in situ* DNP measurements of electrochemical systems, such as lithium-metal based batteries. This MAS frequency independence is in contrast to conventional cross-effect DNP experiments, which generally work best at moderate MAS frequencies [42].

Note that enhancements obtained at close to room temperature using an echo pulse sequence appear significantly larger at lower MAS frequencies; however, this is related to a combination of the strong temperature dependence of the ^{7}Li metal T_{2n} in this temperature range and the sample heating during microwave irradiation (see note S6, Figs. S5 and S6, and discussion below [22]).

We note that the obtained enhancements presented in Fig. 3 vary between the different data sets, even though the same microstructural lithium metal sample was used. We attribute the varying enhancements to slight changes in the microwave power and frequency that are experienced by the sample when using our klystron microwave source. These power and frequency variations may arise from klystron power supply instabilities, temperature fluctuations in the room and the klystron cooling water, and slight changes in the alignment of the microwave transmission line after (re)placing the probe in the magnet. These effects are more noticeable when using a klystron microwave source, as a klystron emits a lower microwave power compared to a gyrotron. Moreover, the narrow lithium metal ESR signal makes the enhancements obtained with this metal more sensitive towards microwave frequency fluctuations compared to those obtained using more typical DNP radicals (see below, Sec. V D). To limit the impact of microwave power and frequency fluctuations on our measurements, each individual data set was acquired within one day; however, different data sets may have been acquired on separate days. The B_0 was optimized prior to each measurement (see above, Sec. III B) to account for any changes in the microwave frequency.

5. T_{1n} vs temperature

The ^{7}Li spin-lattice relaxation time constant (T_{1n}) of the microstructural lithium metal sample was measured as a function of temperature (Fig. 4) in order to estimate the leakage factor (see discussion in Sec. V B 2.). The measured T_{1n} values are inversely proportional to temperature, both with (red) and without (blue) microwave irradiation where the line of best fit has a slope of ∼43.7 and ∼40.6, respectively, which is consistent with previously published work ($T_{1n} = 43.4/T$) [33]. Hence, the nuclear spin-lattice relaxation follows the Korringa relationship over the measured temperature range (100–300 K) at 9.4 T, indicating that nuclear relaxation almost

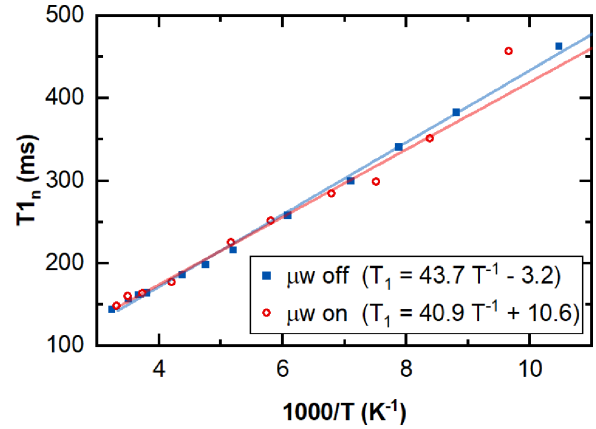

FIG. 4. The ^{7}Li spin-lattice relaxation time constant (T_{1n}) of lithium metal as a function of inverse temperature, recorded with (red) and without (blue) 5.2 W of microwave irradiation at 9.4 T and in a 3.2 mm sapphire rotor at 8 kHz MAS. The T_{1n} values were measured using a saturation-recovery pulse sequence. The sample temperature was determined from the ^{79}Br T_1 and chemical shift of KBr [38]. The lines of the linear best fit for both data sets are shown.

exclusively arises from the interaction with the conduction electrons. The apparent T_{1n} does not change noticeably on application of microwave irradiation, meaning that the DNP buildup time is the same as the T_{1n}, as both are determined only by cross-relaxation with conduction electrons.

The slight deviation from the Korringa relationship for the measurement with microwave irradiation (red) is ascribed to inaccuracies in determining the temperature based on the ^{79}Br chemical shift (for room temperature experiments) and T_{1n} (for ∼100 K experiments) of KBr [38] (with which the sample was diluted), due to uneven heating throughout sample by the microwave irradiation. No evidence for a contribution from the diffusional motion of the lithium spins to the relaxation mechanism was detected in the temperature range studied here. A T_{1n} minimum was previously observed at approximately 383 K at a lower magnetic field strength corresponding to a Larmor frequency of 9 MHz for ^{7}Li (∼0.54 T). Assuming that the source of the T_{1n} minimum is dominated by fluctuations in the ^{7}Li homonuclear coupling driven by the diffusional motion of the lithium atoms (with an associated correlation time of τ_D), a T_{1n} minimum is expected at approximately 0.6 ω_0; the T_{1n} minimum will, therefore, shift to lower temperatures at lower magnetic fields, as the nuclear Larmor frequency increases correspondingly. Consistent with this, the temperature of the T_{1n} minimum dropped to approximately 328 K for a ^{7}Li Larmor frequency of 450 kHz [30,43]. Thus, at the field strengths used here, a contribution from motion to the T_{1n} might be expected even at these high field strengths, but at higher temperatures than studied here (but which could arise for example from high-power microwave irradiation). By contrast, the minimum in the T_{2n} of ∼0.32 ms seen at ∼275 K is likely associated with slow lithium motion (see note S6 [22]). Note that the strong dependence of T_{2n} on temperature is the source of the anomalously high value of ε seen above for slow spinning speeds when an echo sequence is employed: the r.f. heating caused by the microwave results in a noticeably longer T_{2n} (see Fig. S6 [22]), resulting in an

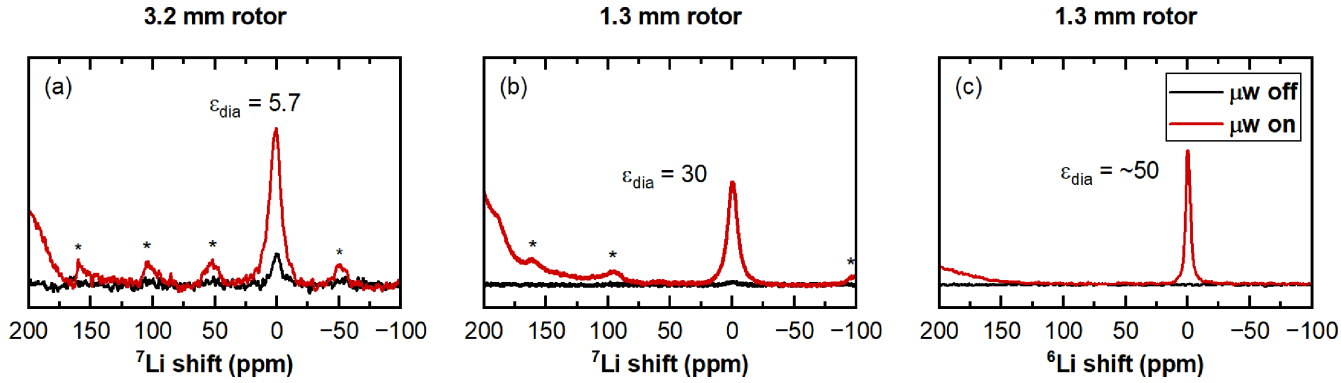

FIG. 5. Expanded view of ^{7}Li NMR spectra shown in Figs. 2(a), 2(b), and 2(c), highlighting the enhancement of the diamagnetic signal: ^{7}Li NMR spectra of microstructural lithium metal without (black) and with (red) 5.2 W of microwave irradiation at 264.6 GHz recorded at 9.4 T and a sample temperature of ∼300 K using a (a) 3.2 mm sapphire rotor at 8 kHz and (b) 1.3 mm zirconia rotor at 15 kHz. Spinning sidebands are marked with an asterisk. The spectra above were acquired with a 1 s recycle delay and took ∼16 s to record.

increase in signal intensity in the echo experiment. This effect is more pronounced at slow MAS due to the longer evolution and refocusing periods used.

B. Diamagnetic lithium signal

Irradiation of the lithium metal CESR also results in the enhancement of the diamagnetic lithium signal: ^{7}Li signal enhancements of ∼5.7 and ∼30 are obtained at room temperature for the same lithium sample packed in a 3.2 and 1.3 mm rotor, respectively [Figs. 5(a) and 5(b)]. The ^{6}Li signal is enhanced by at least 50 [Fig. 5(c)], but the exact determination is challenging due to the low signal intensity in the absence of microwave irradiation. These results show that it is possible to hyperpolarize spins across the metal and nonmetal interface, as reported before [3]. This raises the questions: via what mechanism and how far across the interface can the hyperpolarization be transferred? To address these questions, we will first present the dependence of the diamagnetic signal enhancement on various experimental parameters including temperature, followed by further EXSY experiments to probe the hyperpolarization mechanism in more detail.

1. Enhancement vs applied magnetic field strength

The field profile of the enhancement of the diamagnetic signal [Fig. 6(a)] follows the same trend as the one for the metallic signal [Fig. 3(a)]. This shows that, just like for the metal spins, the hyperpolarization of the diamagnetic lithium spins is achieved via an Overhauser mechanism where the ZQ rate dominates over the DQ rate (giving rise to a positive enhancement). However, we cannot tell from the field profile alone whether the enhancement comes from direct cross-relaxation with the conduction electrons or via an interaction with the metallic ^{7}Li spins (spin diffusion and/or chemical exchange; Fig. 7).

2. Enhancement vs MAS frequency

The enhancement of the ^{7}Li diamagnetic signal generally decreases (albeit only slightly and with pronounced fluctuations) at higher MAS frequencies [Fig. 6(b)]. This is largely consistent with signal enhancement that involves ^{7}Li - ^{7}Li spin diffusion processes, which distribute the hyperpolarization from lithium salts at the lithium metal interface; this process is less efficient at faster spinning frequencies [44]. While slower MAS frequencies—or even static conditions—may yield higher DNP enhancements for the diamagnetic signal, faster MAS frequencies can still be advantageous for achieving higher spectral resolution and for avoiding local heating of the metallic sample during microwave irradiation.

3. Enhancement vs recycle delay

The enhancement of the ^{7}Li diamagnetic signal shows a strong dependence on the recycle delay used [Fig. 6(c)]: shorter recycle delays yield weaker signals but significantly higher enhancements. Figure 6(d) reveals that the diamagnetic signal consists of two components, where the signal at ∼3.2 ppm builds up faster in intensity than the signal at ∼1.1 ppm with increasing length of the recycle delay. This is further supported by T_{1n} relaxation measurements, which required a two-component fit: the fast-relaxing component at ∼3.2 ppm has a $T_{1n} = 0.8$ s, whereas the slow-relaxing component at ∼1.1 ppm has a $T_{1n} = 44$ s. The latter T_{1n} value is similar to that measured for diamagnetic lithium salts (e.g., Li_2CO_3, LiOH, etc.) and is attributed to diamagnetic lithium spins farther from the metal surface, their signal building up more slowly, presumably via spin diffusion. The former is ascribed to diamagnetic spins in proximity to the metal surface, where coupling with the nearby electronic spins provides more efficient relaxation mechanisms, reducing the T_{1n}. The high enhancements obtained with short recycle delays ($\varepsilon > 80$ for 0.1 s recycle delay) reveal that the spins with a shorter T_{1n} (in close proximity to the metal surface) experience a larger degree of hyperpolarization than those with longer T1ns (likely farther from the metal surface). The absolute signal for a 0.1 s recycle delay is still very small, even with microwave irradiation. Note that the higher frequency peak at ∼3.2 ppm is consistent with a lithium environment with a lower coordinate environment (e.g., tetrahedral sites such as those found in Li_2O) and/or an environment that experiences a weak hyperfine/Knight shift due to its close proximity to the lithium metal.

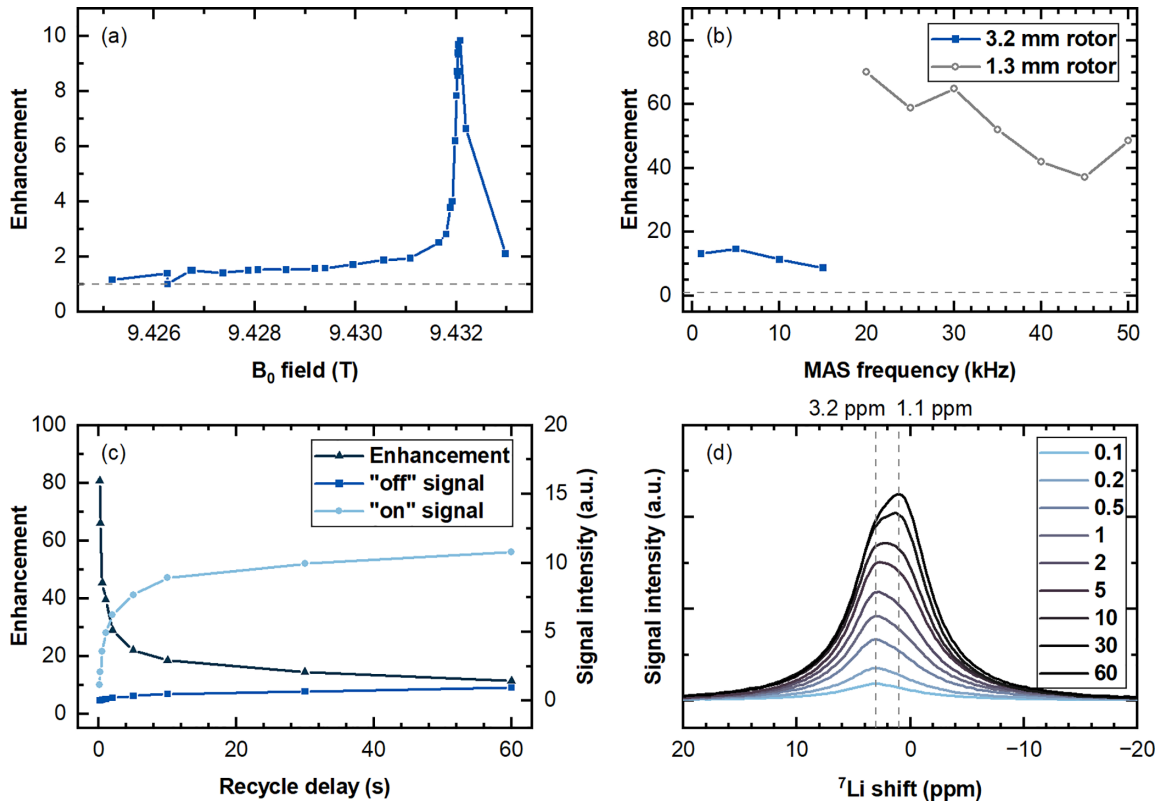

FIG. 6. Enhancement of the diamagnetic ^{7}Li NMR signal of microstructural lithium metal as a function of (a) B_0 field, measured on a 9.4 T magnet, (b) MAS frequency, shown for a 3.2 mm sapphire (blue) and 1.3 mm zirconia (gray) rotor, and (c) recycle delay; the intensity of the diamagnetic ^{7}Li NMR signal acquired with ("on" signal) and without ("off" signal) microwave irradiation are also shown. (d) Diamagnetic region of ^{7}Li NMR spectra acquired with various different recycle delays (0.1–60 s). Unless stated otherwise, all spectra were acquired with 5.2 W of microwave irradiation at 264.4 GHz, on a 9.4 T magnet using a 3.2 mm sapphire rotor at 30 kHz MAS and ∼300 K.

4. Exchange correlation spectroscopy

Two possible routes for the polarization transfer from the conduction electrons to the diamagnetic lithium spins are shown in Fig. 7: the first route requires magnetization transfer from the hyperpolarized metallic lithium spins to the diamagnetic lithium spins (blue arrows), while the second route involves direct cross-relaxation of the diamagnetic lithium spins with the conduction electrons (red arrow). DNP-enhanced two-dimensional exchange correlation spectroscopy (EXSY) experiments were next performed to probe magnetization transfer (in principle via chemical or spin diffusion) between the diamagnetic and metal signals, and to investigate the origin for the *spread* of the metallic lithium signal to lower frequencies upon microwave irradiation. The ^{7}Li EXSY spectrum is shown in Fig. 8(a): the cross-peaks between the metal (∼270 − 230 ppm) and the diamagnetic (0 ppm) signals indicate that there is magnetization transfer between these environments. All parts of the metal signal (including the "tail") correlate with the diamagnetic signal (see top-left cross-peak between metal and diamagnetic signal).

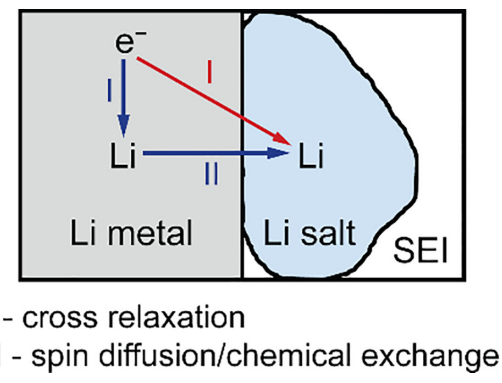

FIG. 7. Schematic of the metal/SEI interface showing possible hyperpolarization routes for the diamagnetic spins.

Figure 8(b) shows an expanded view of the lithium metal EXSY signal shown in Fig. 8(a). The metal cross-peak signal shows signs of T_{2n} broadening, which is consistent with the short T_{2n}. The absence of any significant cross-peak intensity between the most intense part of the metal signal and its contributions at lower frequencies shows that there is little to no spin diffusion or chemical exchange between the lithium environments that make up the "tail" of the metal signal. This is consistent with each individual particle being uniformly hyperpolarized (see Sec. II C 1), with little exchange between the individual particles. This, together with the observation that each part of the metal signal correlates with the diamagnetic signal, suggests the lithium motion and/or spin diffusion is limited to within each individual metal dendrite and its SEI.

A wider range of EXSY experiments were performed at both room and low temperature to explore the transfer of magnetization across the interface (see SM note S7 [22]).

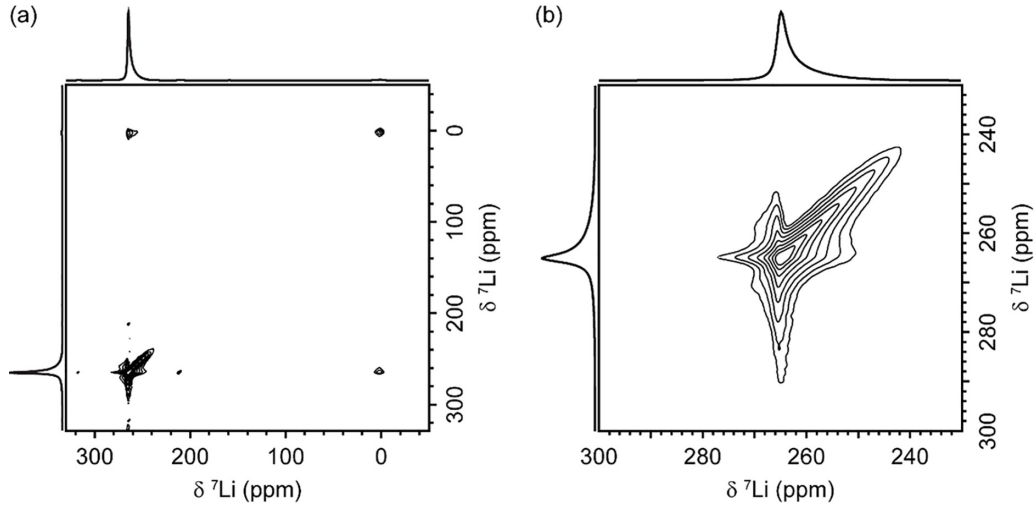

FIG. 8. (a) ^{7}Li EXSY spectrum recorded with 15.6 W microwave irradiation at 14.1 T and room temperature, using a 3.2 mm rotor, a MAS rate of 12.5 kHz and a mixing time of 100 ms, and (b) an expanded region of the EXSY spectrum showing the metallic lithium signal.

Experiments with a mixing time of 200 ms at room temperature and 100 K are compared in Fig. 9. Cross peaks originating from exchange between the lithium metal and the diamagnetic signal are observed with ratios of 15:1 and 4:1 for the lithium metal diagonal:SEI cross-peak at low and room temperature, respectively [Fig. 9(c)]. The weaker cross-peaks at low temperature are consistent with the reduced (or, more likely, lack of) chemical exchange between the lithium metal and the SEI, reduced exchange having been seen previously in related systems [45,46]. At low temperature (100 K), very little if no chemical exchange is expected, and thus the weak cross-peak intensity is ascribed to spin-diffusion across the metal-diamagnetic lithium interface.

C. Overhauser DNP on metallic sodium

To explore the application of Overhauser DNP to other metals, a microstructural sodium sample was prepared. As for lithium, the ^{23}Na NMR spectrum reveals two signals; the main signal at ∼1120 ppm is attributed to the metallic sodium spins, and a minor signal at ∼0 ppm is ascribed to sodium salts in the sample [Fig. 10(a), black; see Fig. S8 for enlarged spectrum [22]). The much larger Knight shift observed for sodium (∼1120 ppm) compared to lithium (∼270 ppm) is due to a larger density of states at the Fermi level [47]. Upon microwave irradiation, only a modest enhancement of ∼1.15 is obtained for the metallic sodium signal at room temperature [Fig. 10(a), inset]. Intriguingly, the Knight shift increased by 1.1 ppm, which is opposite to what is observed for lithium and what might be expected (i.e., irradiation of the sodium CESR reduces the electron spin magnetization, leading to a reduction in the Knight shift). Instead, we attribute the Knight shift increase to the temperature dependence of the sodium Knight shift ($\Delta K = 0.11\frac{ppm}{T}$) [48], which results from volume changes. At larger enhancements, we would still expect a reduction of the Knight shift, analogous to the experiments on lithium metal. During microwave irradiation, the sample can heat up by as much as ∼10 K, which may explain the observed increase in Knight shift of 1.1 ppm. The B_0 field dependence of the enhancement of the metallic sodium signal shows a positive enhancement [Fig. 10(b)], approximately at the B_0 field where $\omega_{\mu w} = \omega_{Na,\,CESR}$, indicating that the sodium signal is also enhanced via an Overhauser mechanism where the ZQ relaxation dominates. The field position

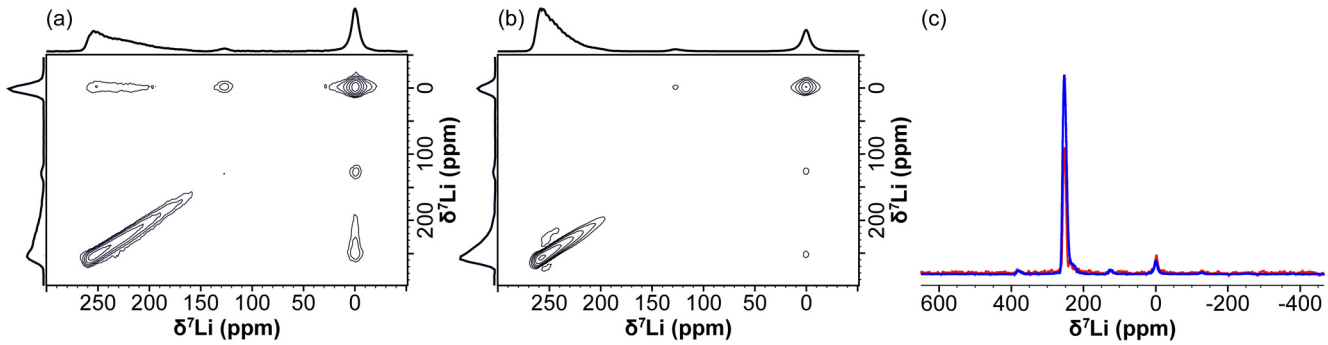

FIG. 9. ^{7}Li EXSY spectrum recorded with 5.2 W microwave irradiation at 9.4 T at (a) room temperature and (b) 100 K, using a 1.3 mm rotor, a MAS rate of 20 kHz, and a mixing time of 200 ms. (c) Slices taken through the lithium metal resonance at low (blue) and room temperature (red). The spectra have been scaled by the Boltzmann factor; the greater intensity of the metallic lithium resonance is ascribed to more efficient enhancement obtained for this low temperature experiment.

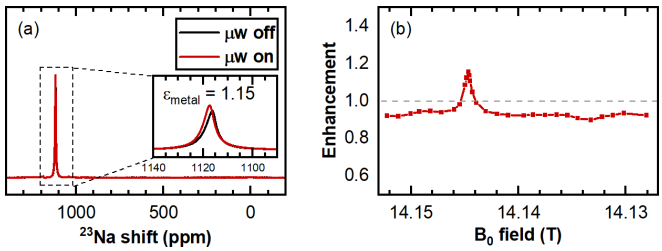

FIG. 10. (a) ^{23}Na NMR spectra of microstructural sodium without (black) and with (red) 395 GHz microwave irradiation recorded at 14.1 T, using a 3.2 mm sapphire rotor at 11.5 kHz and a sample temperature of ∼95 K. (b) Enhancement of the metallic ^{23}Na NMR signal of microstructural sodium metal as a function of B_0 field, measured on a 14.1 T magnet.

at which maximum enhancement is obtained is higher than that for lithium (∼14.105 T on the same DNP system [3]), reflecting the smaller g-factor of sodium metal compared to lithium metal [49,50]. The lower enhancement observed for sodium (∼1.15) compared to lithium (∼10) is attributed to the shorter electronic relaxation times of sodium (see Sec. V C 1). As the electronic relaxation times in sodium metal increase with decreasing temperature, lower temperatures and higher microwave powers are expected to improve the enhancement. Improvements in sample preparation (e.g., sodium concentration in sample, particle size, etc.) may also lead to greater enhancements. It is unclear why the "enhancement" drops below 1 for experiments performed farther than 2 mT from the optimal B_0 field.

V. DISCUSSION

The results presented in this work are now used to gain a deeper understanding of the hyperpolarization mechanism and its (experimental) requirements. First, we rationalize the temperature dependence of enhancement on lithium metal. Next, we discuss why the observed enhancement on lithium metal is significantly lower than the theoretical maximum enhancement and suggest potential routes to improve the experimentally obtained enhancements. We then consider the diamagnetic lithium signal enhancement; this is followed by a reflection on the possible application of Overhauser DNP to conductive samples other than metallic lithium. Finally, we present some considerations regarding the hardware used for DNP experiments on lithium metal at high field strengths.

A. Temperature-(in)dependent enhancement on lithium metal

The largely temperature-independent enhancement is ascribed to the electron relaxation times (T_{1e} and T_{2e}) of lithium metal being essentially temperature independent (see also Sec. V C 1) [24]; thus, the ability to saturate the lithium ESR transition is expected to be independent of temperature [Eq. (9)]. The slightly greater enhancement often—but not always—seen at room temperature may have a mechanistic origin (e.g., change in nuclear relaxation mechanism; see below) or a technical origin (e.g., more efficient microwave coupling at room temperature), or arise from a variety of yet unexplored phenomena including the skin effects (e.g., shorter skin depths at lower temperatures due to a change in resistivity [51,52] and skin effects at the "sample" level due the particle agglomerates). This temperature dependence is in contrast with "standard" DNP radical sources (e.g., TEKPol, AMUPol, etc.), for which the electron relaxation times decrease drastically with increasing temperature and thus appreciable enhancements can be obtained only at low temperatures (<120 K). It also constitutes another advantage of lithium metal DNP experiments, removing the need for costly and technically challenging sample cooling. Note that due to the strong temperature dependence of the ^{7}Li metal T_{2n} at room temperature (see Sec. IV A 5), realistic evaluation of lithium metal signal enhancements at room temperature and 9.4 T should be conducted using one-pulse excitation, sufficiently fast MAS frequencies (⩾10 kHz) or careful calibration of temperatures.

B. Low experimental enhancements

Even though noticeable enhancements of the metallic ^{7}Li NMR signal are achieved (∼10 and ∼50 for lithium metal using a 3.2 mm and 1.3 mm rotor, respectively), these are much lower than the theoretically predicted maximum enhancement for ^{7}Li, given by $\gamma_e/\gamma_{^7Li} \approx 1700$, and lower than the values obtained at very low magnetic fields of 0.03–0.33 T [2,27,32]. Only 0.8% and 3.3% of the theoretical enhancement have been achieved using a 3.2 mm and 1.3 mm rotor, respectively. Similarly modest enhancements are observed for the ^{6}Li (∼147 using a 1.3 mm rotor; *cf.* theoretical maximum $\gamma_e/\gamma_{^6Li} \approx 4500$) and ^{23}Na NMR signals (∼1.15 using a 3.2 mm rotor; *cf.* theoretical maximum $\gamma_e/\gamma_{^{23}Na} \approx 2500$).

As discussed above, the parameters that describe the observed signal enhancement [Eq. (6)] are the coupling, leakage, and saturation factor [Eqs. (3), (7), and (8), respectively]. The theoretical maximum enhancement is achieved when all parameters are equal to 1 (or −1 for the coupling factor). To understand why such relatively small enhancements are achieved experimentally, these factors are evaluated for metallic lithium in the following sections.

Previous studies report a convenient method for determining the saturation factor, which can then be used to calculate the leakage factor, by extrapolating to the maximum practical enhancement: the ordinate intercept of $\frac{1}{\varepsilon}$ vs $\frac{1}{(B_{1,e})^2}$ yields the maximum enhancement for complete saturation of the CESR signal $[(B_{1,e})^2 \to \infty,\ s = 1]$ [6]. However, this method neglects the Overhauser shift of the CESR frequency, observed for high levels of electron spin saturation (see below, Sec. V B 4), often leading to large errors in the determination of the maximum enhancement as well as the coupling, leakage, and saturation factors [8,53]. A modified equation may be used when the electron saturation is sufficiently low (i.e., no noticeable Overhauser shift), but this requires a proportionality factor (x) to convert the applied microwave power (W) to a microwave field experienced by the sample to ($W = x(B_{1,e})^2$). Instead, we will evaluate each parameter individually via methods outlined in the following three sections for ^{7}Li, ^{6}Li, and ^{23}Na, after which the Overhauser shift is considered.

1. Coupling factor

The coupling factor *(ξ)* captures the time-dependent parts of the scalar and dipolar hyperfine interactions. In the case of lithium and sodium metal, the conduction band is a hybrid $s + p$ band, where the electron density at the nucleus is sufficiently large that the contribution of the dipolar hyperfine interaction can be ignored (note this is the case for all alkali metals) [17]. Thus, the hyperfine interaction in both lithium and sodium metal (and other alkali metals) is of the scalar kind, and hence only the ZQ transition is allowed (i.e., $W_0 \neq 0$, $W_1 = W_2 = 0$). Therefore, the equation describing the coupling factor (3) is reduced to $\xi = \frac{-W_0}{W_0}$, and the coupling factor is -1, and therefore does not limit the DNP enhancement [17]. In this case, the coupling factor is expected to be independent of the applied magnetic field strength, B_0, the applied microwave power, $B_{1,e}$, and temperature. Note that this is in stark contrast with cases where the electron-nucleus interaction is mediated via a dipolar coupling (as is common in liquids), as here, the coupling factor has a strong dependence on B_0 and temperature [8,13].

2. Leakage factor

The leakage factor (f), i.e., the rate of nuclear relaxation caused by coupling to the electron relative to the total nuclear relaxation rate, can be determined by measuring and comparing the T_{1n} in the absence and presence of an extrinsic radical source, a method which is used in solution-state Overhauser DNP [18], However, this is not possible for samples where the radical is "native" or intrinsic to the sample. Instead, we exploit the different temperature dependencies of the various nuclear relaxation mechanisms for assessing the leakage factor in lithium metal.

The temperature dependence of the T_{1n} of lithium metal follows the Korringa relation (Fig. 4), which demonstrates that the nuclear relaxation arises from the interaction with the conduction electrons, with little observable contribution from a dipolar mechanism (due to mobile ^{7}Li atoms) at and below room temperature. Therefore, the leakage factor is taken to be close to 1 over the measured temperature range (100–300 K) at 9.4 T and is not a major limiting factor for the DNP enhancement in our experiments. Note, however, that the leakage factor is expected to decrease for much lower B_0 field strengths (especially for $B_0 \ll 1$ T) and at higher temperatures, as the contribution of the dipolar relaxation mechanism to the nuclear relaxation increases [43].

The leakage factor is also expected to be close to 1 for ^{6}Li and ^{23}Na, as the T_{1n} has been shown to follow the Korringa relation [43]. These earlier T_{1n} measurements were performed at low B_0 field strengths (0.9 T for ^{6}Li and 0.3–0.8 T for ^{23}Na), and it may be valuable to repeat these at stronger B_0 fields.

3. Saturation factor

The degree of saturation of the EPR resonance is quantified via the saturation factor (s). Given that the coupling and leakage factors are estimated to be close to -1 and 1, respectively, insufficient electron saturation appears to be the main limiting factor for achieving higher enhancements.

The average saturation factor (for all lithium metal particles) can be estimated from the enhancement, using Eq. (6), assuming $\xi = -1$ and $f = 1$ as discussed above. Using the same data shown in Fig. 2, where an enhancement of ∼13.2 was obtained using the 3.2 mm rotor, this corresponds to a saturation factor of ∼0.0072, while an enhancement of ∼56 was obtained with the 1.3 mm rotor for the 1.3 mm rotor, giving a saturation factor of ∼0.032.

The saturation factor can also be estimated from the reduction of the lithium metal Knight shift (2.3.2) under microwave irradiation (see SM note S9 [22]). For the ^{7}Li NMR spectra acquired with a 3.2 mm sapphire rotor [Fig. 2(a)], the lithium metal signal maximum decreases by 2.07 ppm ($\delta_K - \delta_{Li,ON} = 264.50 - 262.43$ ppm), which corresponds to a saturation factor of ∼0.0078. A similar analysis for the ^{7}Li NMR spectra recorded with a 1.3 mm zirconia rotor [Fig. 2(b)] yields $s \sim 0.023$ ($\delta_K - \delta_{Li,ON} = 6.13$ ppm). If we consider both the spread of and shift of the resonance to lower frequencies (i.e., if we consider the change in the overall line shape), a more accurate average of the overall saturation in the sample is obtained of s ∼ 0.0116 for the 3.2 mm rotor and s ∼ 0.032 for the 1.3 mm rotor (see the SM for details [22]). The breadth of the linewidth provides a measure of the distribution of microwave power seen by the different parts of the sample.

Both methods for estimating the saturation factor are in reasonable agreement and based on these estimations, the lithium metal conduction electron saturation is only 0.7%–0.8% in the 3.2 mm rotor and 2.3%–3.2% in the 1.3 mm rotor; this confirms that the very low degree of electron saturation severely limits the experimental enhancement. The higher degree of saturation obtained with the 1.3 mm probe is consistent with the higher enhancements obtained with the latter and the improved microwave waveguide coupling in the 1.3 mm DNP probe [39]. The agreement between the two estimates of the saturation factor also confirms that the coupling and leakage factor are close to -1 and 1, respectively. Moreover, if the enhancement was limited by the coupling or leakage factor, the enhancement would not be expected to depend on the rotor size used.

The values for s obtained above are only an estimation: the leakage factor, while certainly close to 1, may not be exactly 1, leading to an underestimation of the saturation factor when calculated through Eq. (6). Second, this method is very sensitive to correct chemical shift referencing and the determination of $\delta_{Li,ON}$ and $\delta_{Li,OFF}$, as a difference of 0.1 ppm already corresponds to a change of s of ∼0.0004.

Using the same approaches to analyze the ^{6}Li data [Fig. 2(c)], the saturation factors of ∼0.023 (based on Knight shift reduction of 6.09 ppm) or ∼0.035 for the full line are estimated. As expected, these values are comparable to those achieved for ^{7}Li, especially considering the more notable spread of the line to lower ppm values. These considerations are consistent with the observation that the ^{6}Li and ^{7}Li NMR enhancements obtained on the same lithium sample differ only by the ratio of their gyromagnetic ratios (discussed above), highlighting that the hyperpolarization mechanism and parameters for ^{6}Li and ^{7}Li are very similar and that the enhancements obtained for ^{6}Li are also strongly limited by the degree of electron saturation.

For sodium, the saturation factor cannot be estimated by measuring the Knight shift reduction, as the ^{23}Na NMR signal is affected by sample heating from microwave irradiation.

Instead, the saturation factor is calculated to be ∼0.00006 using Eq. (6) (*cf*. ∼0.007 − 0.008 for ^{7}Li). This suggests that the saturation achieved for sodium is over 100 times smaller compared to lithium, consistent with the shorter electron relaxation times of sodium metal (see Sec. V C 1).

4. The Overhauser shift

We now discuss for completeness a phenomenon that may become important at much higher microwave powers and larger saturation factors. As noted by Overhauser in his original publication, it may be challenging to reach the maximum theoretical enhancement predicted for an OE DNP mechanism on metals, due to the difficulty in achieving complete electron spin saturation when using fixed-frequency microwave sources [1]. As higher degrees of electron saturation are achieved, the resulting increased nuclear polarization now produces a more appreciable (but still small) magnetic field (B_n), which arises from the coupling between the nuclear spins and the unpaired electron spin density; this is analogous to the Knight shift of nuclear spins [1,2,54] where net magnetization of the electron spins results in a local field experienced by the nuclear spins (see Sec. II C 2). The B_n field now experienced by the electron spins shifts their resonance to higher frequencies (for $\gamma_n > 0$). This frequency shift is referred to as the Overhauser shift [6] (or Day shift [27,32,55]) and has been observed experimentally in low-field (∼0.3 T) ESR experiments on lithium metal [27,54].

In the context of conventional high-field DNP experiments with fixed microwave frequency, this phenomenon means that beyond a critical value of saturation, the electron resonance will be shifted too far to where it no longer matches the microwave frequency. At this point, the nuclear polarization will decrease, until B_n is sufficiently small again, so that the electron spin resonance falls within the frequency range of the microwave source. An equilibrium between nuclear polarization and electron saturation will eventually be reached, defining a maximum practical enhancement for a fixed-frequency microwave source and fixed applied magnetic field. The additional magnetic field caused by fully hyperpolarized ^{7}Li spins has been calculated as 21 mT by Overhauser [1], which corresponds to a field change of 2234 ppm or ∼589 MHz change of the lithium conduction electron resonance at $B_0 = 9.4$ T. This would be far outside the excitation bandwidth of current microwave sources at this field. At very higher powers, the use of frequency-sweepable microwave sources would be beneficial for Overhauser DNP on lithium metal so that the CESR resonance could be followed as it shifts due to nuclear hyperpolarization (Overhauser shift), ensuring efficient electron saturation at all times. In principle, magnetic field changes could also be used to "follow" the electron resonance when the microwave frequency remains fixed.

C. Improving experimentally obtained enhancements

The ability to saturate the electron spin transition is strongly affected by the electron relaxation processes, which restore the equilibrium populations. Thus, the degree of saturation can be increased when the relaxation processes are slower (i.e., longer T_{1e} and T_{2e}) and the applied microwave power is greater (i.e., a stronger $B_{1,e}$ field). Additionally, the sample preparation may also play a role in the ability to saturate the electron transition. Below we will discuss several sample and hardware considerations that may improve the experimental enhancements.

1. Electronic relaxation times and their effect on OE enhancements

Lithium metal, with its small spin-orbit coupling, exhibits relatively long (compared to other alkali metals) and temperature-independent electronic relaxation times, with the relaxation mechanism dominated by impurity scattering (see Sec. II C 4). In our previous work we showed that the T_{2e} of electrochemically deposited microstructural lithium is $\sim 2 \times 10^{-7}$ s [3] and longer than that measured previously of 2.5×10^{-8} s for 99.9% purity ($T_{1e} = T_{2e}$ for alkali metals) [24] indicating that our sample preparation method yields high-purity lithium. Preparing samples with even fewer impurities may help reach higher degrees of saturation, and in turn, enhancements, but it may be challenging to obtain such pure samples in practice.

For sodium, the electronic relaxation time increases at lower temperatures changing from T_{2e} values of $\sim 1 \times 10^{-8}$ s at 300 K, to $\sim 3.5 \times 10^{-8}$ s at 80 K and $\sim 1 \times 10^{-7}$ s at 20 K [24,35,36]. This temperature dependence suggests that Overhauser DNP experiments on sodium metal should be performed at the lowest possible temperatures to maximize the enhancement. The T_{2e} of sodium is about an order of magnitude shorter at ∼100 K than that of lithium due to the increased spin-orbit coupling for sodium. This could explain why lower enhancements are achieved for sodium [∼10 for lithium vs ∼1.15 for sodium; Fig. 2(a) vs Fig. 10(a)]: only at temperatures below 20 K does the T_{2e} of sodium become comparable to that of lithium [24]. The electronic relaxation times presented above are taken from low field measurements (∼10 mT for lithium [24] and ∼330 − 860 mT for sodium [35,36]), where the T_{2e} was determined from the CESR line width, thus it may be beneficial to remeasure the electronic relaxation times at the presently used magnetic fields for the lithium metal dendrite samples, which may contain different impurity levels due to different deposition parameters and electrolytes.

2. Microwave source

As electron saturation increases with the strength of the applied microwave field [Fig. 3(d)], a microwave source delivering higher power microwave irradiation to the sample will certainly improve the experimental enhancements. The microwave field experienced by the sample with a klystron microwave source was estimated from the saturation factor and Knight shift reduction using Eq. (9), yielding a field strength of $B_{1,e} = 1.79 \times 10^{-6}$ T. Although this is low for a pulsed-field EPR spectrometer [56], it is comparable to values reported for CW EPR spectrometers operating at W and G bands [57]. This suggests that higher saturation levels may be achievable.

While a gyrotron microwave source nominally provides higher power microwave irradiation (up to ∼50 W) [58] compared to a klystron microwave source (up to ∼5 W) [37],

no noticeable gains in enhancement were observed: repeating the experiments shown in Fig. 2(a) on the same sample and under the same conditions (i.e., room temperature, 3.2 mm rotor) using a gyrotron source ($B_0 = 14.1$ T) gives only an enhancement of ∼11, compared to ∼13 when using a klystron source ($B_0 = 9.4$ T; see note S10 [22]). However, the comparison between the two microwave sources is not trivial, as any microwave losses during transmission may greatly influence the microwave field experienced by the sample. This suggests that, in addition to the power output of the microwave source, the efficiency of microwave delivery to the sample can be a limiting factor in practice. Improvements in the microwave coupling to the sample may, therefore, represent a complementary strategy to boost DNP enhancements.

Further experiments are also required to explore the role that frequency stability with both these microwave sources plays in limiting lithium metal enhancement (see below). No higher-power microwave sources have been developed yet for DNP experiments at the high fields discussed here ($B_0 \geqslant 9.4$ T), but the development of such microwave systems may enable greater enhancements to be achieved for Overhauser DNP. As noted above, pulsed and/or frequency-sweepable microwave sources would also be beneficial to "follow" the electron resonance frequency (Overhauser shift) during Overhauser DNP experiments.

Alternatively, efficient, stable microwave sources are available at lower B_0 fields, which may explain why impressive enhancements of ∼100 have been reported for lithium metal measured at 0.03–0.33 T [2,27,32]. Moreover, lower B_0 field strengths have the advantage of improved skin effects. However, spectra acquired at these low B_0 fields also suffer from poorer S/N and poorer spectral resolution.

3. Microwave penetration into the sample

Another approach for increasing the $B_{1,e}$ field strength experienced by the spins is to improve the microwave penetration into the sample. At the individual metal particle level, the skin effects are of the order of the dendrite diameters, resulting in (close to) uniform microwave irradiation throughout one lithium metal particle (see Secs. II C 1 and IV A). However, we now propose skin effects on the "sample-level": particles closer to the rotor walls may attenuate the microwave irradiation, and as a result particles closer to the center of the rotor may experience a weaker $B_{1,e}$ field. This may explain why higher enhancements are obtained for different dilutions of an identical lithium sample with KBr. In addition, particles buried in dendrite agglomerates will also feel reduced microwave powers. This theory may also partially explain why higher enhancements are obtained when using a 1.3 mm rotor vs a 3.2 mm rotor (lower surface-area-to-volume ratio for the 1.3 mm rotor), even though the improvements made to the microwave transmission in the 1.3 mm probe are most likely responsible for this. We also suggest using smaller particles (and particularly avoiding particles larger than the spin depth), as this will improve skin effects (on both the particle and rotor level), leading to better microwave penetration. Finally, in addition to these skin effect considerations, the dielectric properties of the sample matrix also play a role: KBr has a relatively low dielectric constant, which facilitates microwave propagation into the sample and reduces dielectric losses, thereby contributing to the observed enhancement. Overall, based on our empirical observations, we recommend using high KBr:metal dilution ratios, low sample volumes, and small particles to obtain the highest enhancements.

D. Narrow ESR signal for lithium metal

The narrow width of the lithium metal ESR signal means that the magnetic field range over which $^{6/7}$Li NMR signal enhancements can be achieved is extremely narrow, especially compared to other radical sources used in high-field MAS DNP. Table I shows the widths of the positive enhancement peaks extracted from field sweep profiles at 9.4 T, comparing different unpaired electron sources and DNP mechanisms. For lithium metal, 90% of the maximum enhancement is retained within 0.08 mT of the optimal B_0 field (i.e., $B_0 \pm 0.04$ mT), and 50% is retained within 0.3 mT. For more commonly used DNP radicals, the field range over which appreciable enhancements can be obtained is much wider: 90% of the maximum enhancement is retained within 0.8 mT for the solid effect with 1,3-bisdiphenylene-2-phenylallyl (BDPA; the example with the second-narrowest enhancement peak), which is still ten times wider than that of lithium metal. For 1-(TEMPO-4-oxy)-3-(TEMPO-4-amino)propan-2-ol (TOTAPOL), representative of most bis-nitroxides, this width is even 4 mT, ∼50 times wider than of lithium metal. This demonstrates that the enhancement obtained from lithium metal is much more sensitive towards suboptimal B_0 fields and/or any slight changes in the microwave frequency.

The narrow CESR linewidth has several important consequences for Overhauser DNP experiments on lithium. First, careful field optimization in small steps (we typically used steps of ∼2.3 ppm) is required to find the maximum enhancement. While tedious, this is still a relatively fast process due to the high sensitivity of the (enhanced) lithium metal signal, its short T_{1n} relaxation time, and the use of automation scripts (see Sec. III for more details). Second, the lithium metal signal enhancement is very sensitive to small microwave frequency fluctuations, a phenomenon which we have observed especially for our klystron microwave source. A representative example is given in Fig. S10 [22], where the enhancement fluctuates and slowly decreases to 90% of its maximum value after 4 hours. In contrast, the enhancement remains constant over the same time period when using a gyrotron microwave source (Fig. S10 [22]). The variations in enhancement observed for the klystron are not due to B_0 field drift, as the position of the ^{7}Li NMR resonance remains constant. Instead, we attribute the variation in enhancement to fluctuations in the klystron microwave frequency, which—at least in our system—can arise from small changes in room temperature and the temperature of the klystron cooling water. For a 9.4 T DNP system, a microwave frequency change as small as 1 MHz (∼4 ppm) causes the optimal B_0 field to shift ∼0.04 mT, which would cause the enhancement to drop to ∼90% of its initial value (Table I). While automated hardware approaches for field optimization are possible, particularly with samples with high S/N (by analogy with uses of a "lock" in solution NMR spectroscopy), this can make it challenging to perform longer experiments such as the acquisition of 2D

TABLE I. Width of the positive enhancement peak in the DNP field sweep profile for different DNP mechanisms and unpaired electron sources at 9.4 T (TOTAPOL at 5.0 T).

Nucleus	DNP mechanism[a]	Unpaired electron source	Sample	Width (mT) of the enhancement peak at 50% ε_{max}[b]	Width (mT) of the enhancement peak at 90% ε_{max}[b]	Reference
^{7}Li	OE	Conduction electrons	Li metal	0.3	0.08	This work
^{7}Li	SE	Fe^{3+}	0.5% Fe(III)-doped $Li_4Ti_5O_{12}$	5	1.5	Harchol *et al.* [59]
^{1}H (5 T)	CE	TOTAPOL	Frozen solution[c]	10	4	Song *et al.* [60]
^{1}H	SE	Trityl OX063	Frozen solution[c]	3.5	1.5	Can *et al.* [61]
^{1}H	SE	BDPA	Frozen solution[c]	1.5	0.8	Can *et al.* [61]
^{1}H	OE	BDPA	Frozen solution[c]	2.8	1.2	Can *et al.* [61]

[a]Overhauser effect (OE), solid effect (SE), cross-effect (CE).
[b]Corresponds to the magnetic field range within which at least 50% and 90% of the maximum enhancement are obtained.
[c]Standard sample preparations for testing of DNP radicals. An analyte and the DNP radical are dissolved in a glass-forming, mostly deuterated DNP solvent (e.g., glycerol or water). See references for exact sample composition.

correlation spectra. It is important to emphasize again that these fluctuations of enhancement are quasi-unique to lithium metal Overhauser DNP experiments due to the narrow CESR width of the lithium metal resonance. Such small changes of microwave frequency should not lead to such pronounced and observable intensity changes in DNP experiments with CE radicals (see Fig. S10 for the same experiment on AMUPol [22]) and would most likely also not affect SE or OE effect experiments with other radical sources, such as those listed in Table I. On the other hand, more positively, we could describe lithium metal as an ideal test sample to evaluate the frequency stability of microwave sources in DNP setups. Finally, for higher enhancements, and as already discussed in Sec. V B 4, the change of the CESR frequency through the Overhauser shift mechanism means that the narrow electron resonance is easily "lost" at a fixed microwave frequency.

E. Hyperpolarization mechanism of the diamagnetic spins

One contribution to the hyperpolarization of the diamagnetic spins occurs through magnetization transfer from the metallic lithium spins (Figs. 6 and 8). This magnetization transfer may occur through chemical exchange or through spin diffusion.

One-dimensional EXSY experiments fitted with Bloch-McConnell fits show that the magnetization/chemical exchange rate between lithium metal and the diamagnetic lithium spins in the SEI at close to room temperature ranges from $\sim$1.9−64 s^{-1}, depending on the exact nature of the SEI [45,46]. The exchange rate follows the Arrhenius equation, and thus should slow down significantly at lower temperatures, reducing the hyperpolarization of the diamagnetic signals via this chemical exchange mechanism. This is consistent with the noticeably small cross-peak intensities seen in the 2D EXSY experiments at 100 K [Fig. 9(c)]. However, the enhancement of the diamagnetic spins is comparable at room temperature and 100 K ($\sim$6; see Fig. S11 [22]) in the lithium dendrite systems that we have studied.

Further insights on the polarization transfer mechanism can be obtained by comparing the ratio of the enhancement of the diamagnetic signal to the metal signal obtained for ^{6}Li and ^{7}Li (i.e., $\varepsilon_{dia}/\varepsilon_{metal}$ for ^{6}Li versus ^{7}Li). In the case of chemical exchange, this ratio should be the same, whereas for spin diffusion, this ratio is expected to be higher for ^{7}Li due to more efficient spin diffusion between the metal and the SEI [5]. In our work we find that ^{7}Li($\varepsilon_{dia}/\varepsilon_{metal}$)= 30/56 = 0.54 and ^{6}Li($\varepsilon_{dia}/\varepsilon_{metal}$)= 50/147 = 0.34 [Figs. 2b and 2(c) and Figs. 5(b) and 5(c)]. The higher ratio for ^{7}Li compared to ^{6}Li suggests that spin diffusion is involved in the hyperpolarization mechanism of the diamagnetic spins. Moreover, isotopic labeling experiments indicate that the chemical exchange between lithium and the bulk SEI or electrolyte takes minutes to hours [62] and thus would not be expected to make a significant contribution to the hyperpolarization mechanism for diamagnetic spins not directly located at the interface. Thus, we propose that while chemical exchange may play a role, particularly at close to room temperature, and close to the SEI-lithium metal interface, magnetization transfer via spin diffusion also plays a role and will be required to help transport magnetization from the lithium metal-SEI interface farther into the SEI "bulk." For example, experiments performed as a function of recycle delay reveal increased build-up of SEI signals with longer recycle delays, presumably farther from the interface [Fig. 6(c)].

Several important points must be made, however. First, we note that significant polarization of the diamagnetic spins is observed even in the case of ^{6}Li in nonenriched samples (i.e., with natural abundances of only 7.6%), where spin diffusion might be expected to be significantly reduced. Second, a recent paper describing Overhauser DNP experiments in solid state batteries [4], examining transfer mechanisms from lithium metal to the SEI formed at the interface of a ceramic/polymer composite, has argued that chemical exchange is significant on the basis of similar values of $\varepsilon_{metal}/\varepsilon_{dia}$ obtained for ^{7}Li and ^{6}Li. Direct cross-relaxation between the conduction electrons and diamagnetic lithium spins is also possible, requiring a fluctuating interaction between the two types of spins. Whether this coupling is dipolar or scalar in nature affects the magnitude and sign of the enhancement and also determines how far a spin can be from the metal surface and still be hyperpolarized via this mechanism. The nature of the electron-nucleus interaction is captured by the

coupling factor, ξ, which is positive (as seen here) when the rate of cross-relaxation induced by a scalar interaction is greater than that induced by a dipolar interaction, $M_d J_d(\omega_S) - M_s J_s(\omega_S) < 0.8$, [63,64] The scalar interaction requires an overlap of the electron and nuclear wavefunctions to be effective and thus places spatial limitations on the distance between the conduction electrons and the diamagnetic lithium spins. Most likely, only the diamagnetic spins closest to the metal surface can cross-relax with the electron spins via a scalar hyperfine interaction, further transfer again occurring via spin diffusion. Further experiments are in progress to attempt to quantify the role that this mechanism plays in polarization transfer.

The spin diffusion distance depends on the lifetime of the spin state, the concentration of lithium spins, and the strength of the dipolar coupling between the spins. Assuming an average spin lifetime of diamagnetic ^{7}Li spins, T_{1n}, of ∼0.8 s at room temperature and a spin diffusion rate of 80 nm^2/s estimated for a dense lithium ceramic (lithium titanate) [65], the hyperpolarization should be transferred ∼8 nm away from the metal surface, before the magnetism decays. This indicates that only the spins within a certain proximity to the metal surface will be hyperpolarized and can be selectively probed using Overhauser DNP. In our system, the spins farther away have longer T_{1n} times and thus polarization transfer may occur out to longer distances. A smaller spin diffusion rate of 5.3 nm^2/s was estimated for ^{6}Li, but these spins also have much longer T_{1n} times of many seconds, indicating that spin diffusion will also play a role in transporting the magnetization from the interface. We stress that these diffusion rates were estimated for static systems, and the experiments here are performed under MAS where the homonuclear coupling will be partially quenched. A small reduction in enhancement of the diamagnetic signal is seen as the MAS rate is increased, but the trend is masked by the much higher microwave coupling associated with the fast MAS probe [Fig. 6(b)].

These estimates for the extent to which the diamagnetic signal is enhanced will have implications when using Overhauser DNP to study the lithium metal surface in lithium metal-based batteries. In these systems, a passivating SEI layer grows on the lithium metal surface, which is formed through the reduction of the electrolyte solution on contact with lithium metal. The SEI is a highly heterogeneous mixed organic/inorganic film of reduction products and has a reported thickness of 10–100 nm on lithium metal [66]. Our present findings on the hyperpolarization mechanism for the diamagnetic lithium spins suggest that only the (lithium-containing) SEI components closest to the metal surface (< approximately 10 nm) are selectively hyperpolarized.

The hyperpolarization of other nuclei on the metal surface would be expected to proceed via an analogous mechanisms and, if chemical or magnetization exchange is the dominant mechanism, would be expected to be less efficient. This is certainly consistent with the little or no ^{1}H (and ^{19}F) enhancement was observed in previous work; however, it should be noted that F- and indeed H-containing species may not (always) be present at these interfaces. Instead, cross-polarization experiments can be used to selectively enhance the signals from nuclei other than lithium, as has previously been shown [3].

F. Application of Overhauser DNP to other conductive solids

We now briefly discuss the possible application of Overhauser DNP to other conductive solids. Based on our results obtained on lithium and sodium metal, it appears that samples of interest should have electronic relaxation times of at least $\sim 10^{-8}$ to 10^{-7} s to achieve adequate levels of saturation for the presently used microwave setups. Nuclear relaxation should also arise predominantly from the interaction with the electronic spins in order to attain any appreciable enhancement.

We start by considering the remaining alkali metals: potassium, rubidium, and cesium have all been shown to follow a Korringa relation [43,67–69]. The electronic relaxation time constants for alkali metals (other than lithium) are inversely dependent on temperature and shorter for heavier metals, due to increased spin-orbit coupling [34]. For example, the T_{2e} for potassium and rubidium are only $\sim 5 \times 10^{-9}$ s [24] and $\sim 3 \times 10^{-9}$ s at 4 K [70], respectively, that for potassium becoming too short to observe an ESR signal at higher temperatures [24]. Electronic transitions with such short relaxation times would be challenging to saturate using the presently available microwave sources, and hence no enhancement from an Overhauser mechanism would be expected. For other pure metals (i.e., no alloys), the nuclear relaxation also tends to follow the Korringa relation (e.g., aluminum [71], magnesium [72], copper [73], and rhodium and palladium [74]), but spin-orbit coupling will also be very large. Additional relaxation mechanisms such as a quadrupolar relaxation mechanism or relaxation induced by paramagnetic impurities may also become more pronounced depending on the temperature and B_0 field, leading to less efficient nuclear-electron cross-relaxation. The conduction bands of these metals have a p/d-character, therefore a dipolar coupling between the nuclear and electronic spins is expected. In this case, W_1 and W_2 are no longer equal to 0, which may affect the coupling factor and lead to smaller enhancements. Like the heavier alkali metals, most other metals have electronic relaxation times that are too short at liquid nitrogen temperatures and are not expected to result in nuclear hyperpolarization (e.g., for copper, the $T_{2e} = 3 \times 10^{-11}$ s at 80 K [75], for aluminum, the $T_{2e} = 5 \times 10^{-10}$ s at 4 K [63,64], and the electronic relaxation times of magnesium, palladium, and tungsten at 4 K are too short for any signal too be observed [24]). The only exception might be beryllium: similar to lithium, the T_{2e} of beryllium is purity-dependent due to the small degree of spin-orbit coupling (spin-orbit coupling representing a major relaxation mechanism). The T_{2e} is $\sim 2 \times 10^{-8}$ s for 4–296 K [24,76], which may be just long enough to observe nuclear hyperpolarization. However, due to the severe toxicity of beryllium metal, experimental verification is strongly discouraged.

Semiconductors also fulfil the requirements for Overhauser DNP, as like metals they have conduction electrons that provide the motion to drive the cross-relaxation of the electron-nucleus couple. Here the conduction electrons observe Boltzmann statistics rather than Fermi statistics (as is

the case for metals), resulting in a smaller electron density in the conduction band [6]. Their lower conductivity, however, results in less pronounced skin effects. While a detailed discussion on the theory of nuclear and electron spin relaxation in semiconductors is outside the scope of this work, we recognize that both nuclear and electronic relaxation in semiconductors are more complex, due to multiple additional relaxation mechanisms [49,77,78] and a complex dependence of the relaxation rate on the nature of the dopant, dopant concentration, temperature, and field strength [79,80]. This may negatively affect the leakage factor depending on the experimental conditions (for phosphorus-doped silicon, a leakage factor of 0.009 was determined at 4.4 K) [81]. On the other hand, the saturation of the electron spin transition in semiconductors may be more efficient compared to metals. The electronic relaxation times can become very long (on the order of μs or even ms) at liquid helium temperatures: for phosphorus doped silicon (6.5×10^{16} cm^{-3} P), the T_{2e} can be as long as 0.2 s at < 1 K and 4.6 T [82,83]. This has led to the successful application of Overhauser DNP on semiconductors [77,84].

With the endless possibilities of semiconductors and metal alloys that have yet to be considered, we are optimistic that there will be other materials suitable for Overhauser DNP. For example, conductive organic polymers may also present a suitable system for Overhauser DNP. For example, recently, enhancements between 24 and 45 were obtained for the ^{1}H and ^{13}C NMR signals from poly acetylene via an Overhauser mechanism at both 100 K and room temperature [85]. Overhauser DNP on graphite has also been demonstrated in early work [86], with more recent studies extending this to lithiated graphite [87].

VI. CONCLUSION

In this work we have systematically investigated the Overhauser DNP effect and its limitations as applied to alkali metals. For a microstructural lithium sample, enhancements of close to 50 and 150 were obtained for ^{7}Li and ^{6}Li, respectively, using a 1.3 mm rotor. Although particle-level skin effects are less severe for the dendrites studied here, the enhancements obtained when using different sample volumes (3.2 vs 1.3 mm rotor) and different degrees of dilution indicate that "skin effects" are seen at the sample level, where microwave penetration into deeper regions of the rotor, and the agglomerated metal particles and/or dendrites is limited. For microstructural sodium metal, only a modest enhancement of 1.15 was obtained (in 3.2 mm sapphire rotor), which is ascribed to the shorter and temperature-dependent electronic relaxation times for sodium.

Following a theoretical treatment of the Overhauser mechanism, we applied this theory to lithium metal to explain why relatively low enhancements are obtained (∼50 compared to a theoretical maximum of 1700 for ^{7}Li). Through a systematic investigation of the enhancement as a function of experimental parameters (B_0, temperature, microwave power, and MAS frequency), we showed that the experimental enhancements are strongly limited by saturation of the electron spin transition. Similar results were obtained for ^{6}Li and ^{23}Na. Despite lithium having the longest electronic relaxation times compared to other alkali metals, the relaxation is still too fast to reach appreciable saturation levels with the present microwave systems. The electron saturation may be improved by using stronger microwave fields, by performing experiments at lower temperatures for ^{23}Na (<80 K) and with samples with fewer impurities (^{7}Li). Sample considerations, such as sample volume, metal particle size, and metal concentration, may also be important for obtaining high enhancements. Overhauser DNP experiments on lithium metal are further complicated by the extremely narrow ESR signal for lithium metal, which makes the enhancement highly sensitive towards the frequency stability of the microwave source. The atoms in lithium metal become highly mobile as the melting temperature is approached, and even at room temperature this mobility affects the T_2^*. Thus, care is needed on applying microwave power to separate sample heating effects from those due to genuine hyperpolarization mechanisms (which may also be temperature dependent).

Studies on the hyperpolarization mechanism of the diamagnetic spins (i.e., nonmetallic lithium) at the interface between lithium metal and the lithium metal passivation (SEI) layer suggest that the magnetization exchange is important; at low temperature spin diffusion is important, but with multiple studies indicating that direct transfer (chemical exchange) can occur at room temperature. Direct enhancement of the diamagnetic lithium signal arising from direct cross-relaxation with the conduction electrons, mediated via a scalar hyperfine interaction, may also occur, but further studies are required to quantify the importance of this mechanism. The hyperpolarization is then transferred to spins farther from the metal surface largely via spin diffusion, allowing ^{7}Li spins within approximately ∼10 nm from the metal surface to be hyperpolarized; the thickness of the region that can be polarized will, however, depend on a number of factors including the density of Li spins in the solid, whether the ^{7}Li ions are mobile, their T_{1n}s and the MAS rates.

Considering other conductive materials for Overhauser DNP, it appears that lithium metal possesses a unique combination of beneficial qualities, making it a highly suitable system for Overhauser DNP. The high enhancements achieved for ^{6}Li (∼150) using a 1.3 mm rotor and a small sample quantity (∼0.2 mg of lithium), are particularly promising because higher resolution ^{6}Li spectra can often be obtained. The development of sweepable high-power microwave sources may enable the application of Overhauser DNP to a wider range of other conductive samples.

ACKNOWLEDGMENT

This work was supported by the Faraday Institution degradation project (FIRG001, FIRG024) and an Advanced ERC Fellowship award to CPG (BATNMR – 835073).

DATA AVAILABILITY

The data that support the findings of this article are not publicly available upon publication because it is not technically feasible and/or the cost of preparing, depositing, and hosting the data would be prohibitive within the terms of this research project. The data are available from the authors upon reasonable request.

[1] A. W. Overhauser, Polarization of nuclei in metals, Phys. Rev. **92**, 411 (1953).

[2] T. R. Carver and C. P. Slichter, Polarization of nuclear spins in metals, Phys. Rev. **92**, 212 (1953).

[3] M. A. Hope, B. L. D. Rinkel, A. B. Gunnarsdóttir, K. Märker, S. Menkin, S. Paul, I. V. Sergeyev, and C. P. Grey, Selective NMR observation of the SEI–metal interface by dynamic nuclear polarisation from lithium metal, Nat. Commun. **11**, 2224 (2020).

[4] A. Maity, A. Svirinovsky-Arbeli, Y. Buganim, C. Oppenheim, and M. Leskes, Tracking dendrites and solid electrolyte interphase formation with dynamic nuclear polarization—NMR spectroscopy, Nat. Commun. **15**, 9956 (2024).

[5] Z. Zhang, J. Tian, J. Chen, Y. He, C. Liu, X. Liang, and J. Feng, Li plating on carbon electrode surface probed by low-field dynamic nuclear polarization ^{7}Li NMR, Chin. Phys. Lett. **38**, 126801 (2021).

[6] A. Abragam, *Principles of Nuclear Magnetism* (Oxford University Press, Oxford, 1961).

[7] A. Abragam, Overhauser effect in nonmetals, Phys. Rev. **98**, 1729 (1955).

[8] K. H. Hausser and D. Stehlik, Dynamic nuclear polarization in liquids, Adv. Magn. Opt. Reson. **3**, 79 (1968).

[9] C. D. Jeffries, Dynamic orientation of nuclei by forbidden transitions in paramagnetic resonance, Phys. Rev. **117**, 1056 (1960).

[10] T. J. Schmugge and C. D. Jeffries, High dynamic polarization of protons, Phys. Rev. **138**, A1785 (1965).

[11] B. Corzilius, High-field dynamic nuclear polarization, Annu. Rev. Phys. Chem. **71**, 143 (2020).

[12] T. V. Can, Q. Z. Ni, and R. G. Griffin, Mechanisms of dynamic nuclear polarization in insulating solids, J. Magn. Reson. **253**, 23 (2015).

[13] I. Solomon, Relaxation processes in a system of two spins, Phys. Rev. **99**, 559 (1955).

[14] M. D. Lingwood and S. Han, Solution-State Dynamic Nuclear Polarization, Annu. Rep. NMR Spectrosc. **73**, 83 (2011).

[15] J. Keeler, *Understanding NMR Spectroscopy*, 2nd ed. (Wiley, Hoboken, 2010).

[16] A. S. L. Thankamony, J. J. Wittmann, M. Kaushik, and B. Corzilius, Dynamic nuclear polarization for sensitivity enhancement in modern solid-state NMR, Prog. Nucl. Magn. Reson. Spectrosc. **102–103**, 120 (2017).

[17] G. R. Khutsishvili, The Overhauser effect and related phenomena, Soviet Phys. Uspekhi **3**, 285 (1960).

[18] V. P. Denysenkov and T. F. Prisner, Liquid-state Overhauser DNP at high magnetic fields, EMagRes **8**, 41 (2019).

[19] A. W. Overhauser, Paramagnetic relaxation in metals, Phys. Rev. **89**, 689 (1953).

[20] R. N. Edmonds, M. R. Harrison, and P. P. Edwards, Conduction electron spin resonance in metallic systems, Annu. Rep. Prog. Chem. C: Phys. Chem. **82**, 265 (1985).

[21] D. R. Lide, *CRC Handbook of Chemistry and Physics* (CRC Press, 2003).

[22] See Supplemental Material at http://link.aps.org/supplemental/10.1103/tpch-2ftn for details on the nutation experiments; SEM images of microstructural lithium samples; discussion of the origin of frequency shift in metals; topspin AU programs for lock field changes and lock field sweeps; ESR spectra of microstructural lithium; the effect of microwave irradiation on the T_{2n} of metallic lithium; exchange spectroscopy (EXSY) experiments; ^{23}Na NMR spectrum; estimation of the saturation factor; and enhancement variation over time.

[23] F. J. Dyson, Electron spin resonance absorption in metals. II. Theory of electron diffusion and the skin effect, Phys. Rev. **98**, 349 (1955).

[24] G. Feher and A. F. Kip, Electron spin resonance absorption in metals. I. Experimental, Phys. Rev. **98**, 337 (1955).

[25] J. H. Pifer and R. Magno, Conduction-electron spin resonance in a lithium film, Phys. Rev. B **3**, 663 (1971).

[26] V. Palenskis, Drift mobility, diffusion coefficient of randomly moving charge carriers in metals and other materials with degenerated electron gas, World J. Condensed Matter Phys. **3**, 73 (2013).

[27] M. Gueron and C. Ryter, Overhauser effect in metallic lithium, Phys. Rev. Lett. **3**, 338 (1959).

[28] W. D. Knight, Nuclear magnetic resonance shift in metals, Phys. Rev. **76**, 1259 (1949).

[29] C. H. Townes, C. Herring, and W. D. Knight, The effect of electronic paramagnetism on nuclear magnetic resonance frequencies in metals, Phys. Rev. **77**, 852 (1950).

[30] R. Messer and F. Noack, Nuclear magnetic relaxation by self-diffusion in solid lithium: T1-frequency dependence, Appl. Phys. **6**, 79 (1975).

[31] D. P. Tunstall, Many-electron enhancement effects on the nuclear spin-lattice relaxation times in metals, J. Magnetic Resonance (1969) **6**, 500 (1972).

[32] R. Hecht and A. G. Redfield, Overhauser effect in metallic lithium and sodium, Phys. Rev. **132**, 972 (1963).

[33] J. Korringa, Nuclear magnetic relaxation and resonance line shift in metals, Physica **16**, 601 (1950).

[34] R. J. Elliott, Theory of the effect of spin-orbit coupling on magnetic resonance in some semiconductors, Phys. Rev. **96**, 266 (1954).

[35] W. Kolbe, Spin relaxation time of conduction electrons in bulk sodium metal, Phys. Rev. B **3**, 320 (1971).

[36] F. Vescial, N. S. Vanderven, and R. T. Schumacher, Spin-lattice relaxation time of conduction electrons in sodium metal, Phys. Rev. **134**, A1286 (1964).

[37] M. Rosay, I. Sergeyev, L. Tometich, C. Hickey, A. Roitman, D. Yake, and D. Berry, Opportunities and challenges for EIK's in DNP NMR applications, *43rd International Conference on Infrared, Millimeter, and Terahertz Waves (IRMMW-THz 2018), Nagoya, Japan* (IEEE, Red Hook, 2018), p. 1290.

[38] K. R. Thurber and R. Tycko, Measurement of sample temperatures under magic-angle spinning from the chemical shift and spin-lattice relaxation rate of ^{79}Br in KBr powder, J. Magn. Reson. **196**, 84 (2009).

[39] A. Purea, C. Reiter, A. I. Dimitriadis, E. de Rijk, F. Aussenac, I. Sergeyev, M. Rosay, and F. Engelke, Improved waveguide coupling for 1.3 mm MAS DNP probes at 263 GHz, J. Magn. Reson. **302**, 43 (2019).

[40] B. M. Meyer, N. Leifer, S. Sakamoto, S. G. Greenbaum, and C. P. Grey, High field multinuclear NMR investigation of the SEI layer in lithium rechargeable batteries, Electrochem. Solid-State Lett. **8**, A145 (2005).

[41] M. A. Antoniades, and G. V. Eleftheriades, and N. M. R. Nomenclature, Nuclear spin properties and conventions for chemical shifts, Pure Appl. Chem. **73**, 1795 (2001).

[42] F. Mentink-Vigier, Ü. Akbey, Y. Hovav, S. Vega, H. Oschkinat, and A. Feintuch, Fast passage dynamic nuclear polarization on rotating solids, J. Magn. Reson. **224**, 13 (2012).
[43] D. F. Holcomb and R. E. Norberg, Nuclear spin relaxation in alkali metals, Phys. Rev. **98**, 1074 (1955).
[44] B. P. Tatman, W. T. Franks, S. P. Brown, and J. R. Lewandowski, Nuclear spin diffusion under fast magic-angle spinning in solid-state NMR, J. Chem. Phys. **158**, 184201 (2023).
[45] R. May, K. J. Fritzsching, D. Livitz, S. R. Denny, and L. E. Marbella, Rapid interfacial exchange of Li ions dictates high coulombic efficiency in Li metal anodes, ACS Energy Lett. **6**, 1162 (2021).
[46] D. Columbus, V. Arunachalam, F. Glang, L. Avram, S. Haber, A. Zohar, M. Zaiss, and M. Leskes, Direct detection of lithium exchange across the solid electrolyte interphase by ^{7}Li chemical exchange saturation transfer, J. Am. Chem. Soc. **144**, 9836 (2022).
[47] B. Mishra, L. K. Das, T. Sahu, G. S. Tripathi, and P. K. Misra, Theory of knight shift in metals, Phys. Lett. A **106**, 81 (1984).
[48] NMR tables, in *Progress in Materials Science*, Vol. 20 (Elsevier, Oxford, 1976), pp. 119–378.
[49] Y. Yafet, g factors and spin-lattice relaxation of conduction electrons, Solid State Phys: Adv. Res. Appl. **14**, 1 (1963).
[50] Y. Yafet, Calculation of the g factor of metallic sodium, Phys. Rev. **85**, 478 (1952).
[51] J. Bass, W. P. Pratt, and P. A. Schroeder, The temperature-dependent electrical resistivities of the alkali metals, Rev. Mod. Phys. **62**, 645 (1990).
[52] T. C. Chi, Electrical resistivity of alkali elements, J. Phys. Chem. Ref. Data **8**, 339 (1979).
[53] W. Buchner and K. H. Hausser, The effect of stimulated emission on the amplification factor in dynamic nuclear polarisation, Z. Naturforsch. A **21**, 2121 (1966).
[54] C. Ryter, Direct measurement of the electron density at the nucleus in metallic lithium at liquid helium temperature, Phys. Rev. Lett. **5**, 10 (1960).
[55] C. P. Slichter, The discovery and renaissance of dynamic nuclear polarization, Rep. Prog. Phys. **77**, 072501 (2014).
[56] G. R. Eaton, S. S. Eaton, R. W. Quine, D. Mitchell, V. Kathirvelu, and R. T. Weber, A signal-to-noise standard for pulsed EPR, J. Magn. Reson. **205**, 109 (2010).
[57] B. Rakvin, D. Carić, and M. Kveder, Enhanced accuracy of the microwave field strength measurement in a CW-EPR by pulsed modulation technique, J. Magn. Reson. **287**, 123 (2018).
[58] M. Rosay, L. Tometich, S. Pawsey, R. Bader, R. Schauwecker, M. Blank, P. M. Borchard, S. R. Cauffman, K. L. Felch, R. T. Weber, R. J. Temkin, R. G. Griffin, and W. E. Maas, Solid-state dynamic nuclear polarization at 263 GHz: Spectrometer design and experimental results, Phys. Chem. Chem. Phys. **12**, 5850 (2010).
[59] A. Harchol, G. Reuveni, V. Ri, B. Thomas, R. Carmieli, R. H. Herber, C. Kim, and M. Leskes, Endogenous dynamic nuclear polarization for sensitivity enhancement in solid-state NMR of electrode materials, J. Phys. Chem. C **124**, 7082 (2020).
[60] C. Song, K. N. Hu, C. G. Joo, T. M. Swager, and R. G. Griffin, TOTAPOL: A biradical polarizing agent for dynamic nuclear polarization experiments in aqueous media, J. Am. Chem. Soc. **128**, 11385 (2006).
[61] T. V. Can *et al.*, Overhauser effects in insulating solids, J. Chem. Phys. **141**, 064202 (2014).
[62] A. J. Ilott and A. Jerschow, Probing solid-electrolyte interphase (SEI) growth and ion permeability at undriven electrolyte-metal interfaces using ^{7}Li NMR, J. Phys. Chem. C **122**, 12598 (2018).
[63] S. Schultz, G. Dunifer, and C. Latham, Observation of conduction electron spin resonance in aluminum, Phys. Lett. **23**, 192 (1966).
[64] D. Lubzens and S. Schultz, Observation of an anomalous frequency dependence of the conduction-electron spin resonance in Al, Phys. Rev. Lett. **36**, 1104 (1976).
[65] S. Björgvinsdóttir, P. Moutzouri, P. Berruyer, M. A. Hope, and L. Emsley, Sensitivity enhancements in lithium titanates by incipient wetness impregnation DNP NMR, J. Phys. Chem. C **124**, 16524 (2020).
[66] E. Peled and S. Menkin, Review—SEI: Past, present and future, J. Electrochem. Soc. **164**, A1703 (2017).
[67] A. Narath and H. T. Weaver, Effects of electron-electron interactions on nuclear spin-lattice relaxation rates and knight shifts in alkali and noble metals, Phys. Rev. **175**, 373 (1968).
[68] H. T. Weaver and A. Narath, Low-temperature pressure-dependence studies of knight shifts and nuclear spin-lattice relaxation rates in cesium and rubidium metals, Phys. Rev. B **1**, 973 (1970).
[69] D. F. Holcomb, J. A. Kaeck, and J. H. Strange, Nuclear spin relaxation in Cs metal, Phys. Rev. **150**, 306 (1966).
[70] R. N. Edmonds, P. P. Edwards, S. C. Guy, and D. C. Johnson, Electron spin resonance in small particles of sodium, potassium, and rubidium metals, J. Phys. Chem. **88**, 3764 (1984).
[71] J. J. Spokasj and C. P. Slichterj, Nuclear relaxation in aluminum, Phys. Rev. **113**, 1462 (1959).
[72] L. H. Zitzman, Nuclear spin relaxation (spin-lattice and spin-spin) in magnesium metal, Ph.D. thesis, University of Illinois at Urbana-Champaign, 1972.
[73] W. W. Warren and W. G. Clark, Knight shift and nuclear spin-lattice relaxation rate in solid and liquid copper, Phys. Rev. B **1**, 24 (1970).
[74] A. Narath, A. T. Fromhold, and E. D. Jones, Nuclear spin relaxation in metals: Rhodium, palladium, and silver, Phys. Rev. **144**, 428 (1966).
[75] R. Magno and J. H. Pifer, Conduction-electron spin-resonance study of bimetallic samples, Phys. Rev. B **10**, 3727 (1974).
[76] G. Feher and A. F. Kip, Electron spin resonance in beryllium, Phys. Rev. **95**, 1343 (1954).
[77] G. Kaur and G. Denninger, Dynamic nuclear polarization in III–V semiconductors, Appl. Magn. Reson. **39**, 185 (2010).
[78] J. A. McNeil and W. G. Clark, Nuclear quadrupolar spin-lattice relaxation in some III–V compounds, Phys. Rev. B **13**, 4705 (1976).
[79] R. K. Sundfors and D. F. Holcomb, Nuclear magnetic resonance studies of the metallic transition in doped silicon, Phys. Rev. **136**, A810 (1964).
[80] A. Honig and E. Stupp, Electron spin-lattice relaxation in phosphorus-doped silicon, Phys. Rev. **117**, 69 (1960).

[81] V. Dyakonov and G. Denniger, Overhauser-shift measurements on Si:P near the metal-insulator transition, Phys. Rev. B **46**, 5008 (1992).

[82] J. Järvinen *et al.*, Efficient dynamic nuclear polarization of phosphorus in silicon in strong magnetic fields and at low temperatures, Phys. Rev. B **90**, 214401 (2014).

[83] G. Feher and E. A. Gere, Electron spin resonance experiments on donors in silicon. II. Electron spin relaxation effects, Phys. Rev. **114**, 1245 (1959).

[84] B. Gotschy and G. Denninger, Overhauser shift and dynamic nuclear polarization in InP, Solid State Commun. **71**, 629 (1989).

[85] Z. Miao, F. J. Scott, J. van Tol, C. R. Bowers, A. S. Veige, and F. Mentink-Vigier, Soliton based dynamic nuclear polarization: An Overhauser effect in cyclic polyacetylene at high field and room temperature, J. Phys. Chem. Lett. **15**, 3369 (2024).

[86] A. Abragam, A. Landesman, and J. M. Winter, Effect Overhauser dans les charbons et graphites, C. R. Acad. Sci. **257**, 1849 (1958).

[87] T. Insinna, A.-L. Barra, and C. P. Grey, Overhauser dynamic nuclear polarization of lithiated graphite anodes: Probing bulk and surface structures, Chem. Mater. **37**, 5167 (2025).